Stomach-derived human insulin-secreting organoids restore glucose homeostasis

Xiaofeng Huang[1], **Wei Gu**[1], **Jiaoyue Zhang**[1], **Ying Lan**[1], **Jonathan L. Colarusso**[1], **Sanlan Li**[1], **Christoph Pertl**[1], **Jiaqi Lu**[1], **Hyunkee Kim**[1], **Jian Zhu**[1], **David T. Breault**[2,3], **Jean Sévigny**[4,5], **Qiao Zhou**[1,*]

[1]Division of Regenerative Medicine & Ansary Stem Cell Institute, Department of Medicine, Weill Cornell Medicine, 1300 York Avenue, New York, NY 10065, USA

[2]Division of Endocrinology, Boston Children's Hospital and Department of Pediatrics, Harvard Medical School, 300 Longwood Avenue, Boston, MA 02115, USA

[3]Harvard Stem Cell Institute, Cambridge, MA 02138, USA

[4]Département de Microbiologie-Infectiologie et d'immunologie, Faculté de Médecine, Université Laval, Québec City, QC G1V 0A6, Canada

[5]Centre de recherche du CHU de Québec – Université Laval, Québec city, QC G1V 4G2, Canada.

Abstract

Gut stem cells are accessible by biopsy and propagate robustly in culture, offering an invaluable resource for autologous cell therapies. Insulin-producing cells can be induced in mouse gut, but it has not been possible to generate abundant and durable insulin-secreting cells from human gut tissues to evaluate their potential as a cell therapy for diabetes. Here we describe a protocol to differentiate cultured human gastric stem cells (hGSCs) into pancreatic islet-like organoids containing gastric insulin-secreting (GINS) cells that resemble β-cells in molecular hallmarks and function. Sequential activation of the inducing factors NGN3 and PDX1-MAFA led hGSCs onto a distinctive differentiation path, including a SOX4[High] endocrine and Galanin[High] GINS precursor, before adopting β-cell identity, at efficiencies close to 70%. GINS organoids acquired glucose-stimulated insulin secretion in 10 days and restored glucose homeostasis for over 100 days in diabetic mice after transplantation, providing proof of concept for a promising approach to treat diabetes.

Gut stem cells are highly proliferative and power the weekly self-renewal of the gut mucosal lining[1–3]. Harvested from biopsies, human gut stem cells can be propagated in culture as organoids or primary cell lines over many generations, providing abundant tissues for potential autologous transplantation therapies[4–6]. Gut stem cells produce gut-specific tissues, including hormone-secreting enteroendocrine cells (EECs). Rare insulin expressing EECs have been reported in fetal human small intestine[7]. Whether such cells secret insulin is unknown, but their presence suggests an intrinsic permissiveness for insulin production in the fetal if not postnatal intestine. Prior to this discovery, it was shown that suppressing FoxO1 could activate insulin in murine intestinal EECs[8] and that pancreatic endocrine-like cells could be generated from putative human endocrine progenitors[9]. We also reported that co-expression of the endocrine regulator NEUROG3 (also known as NGN3) and pancreatic β-cell regulators PDX1 and MAFA could induce insulin-secreting cells from murine intestine and stomach[10,11]. However, the same approaches yielded few insulin producers from human gut organoids[11,12].

Generating functional insulin-secreting cells has tremendous therapeutic value, offering treatments for insulin-dependent diabetes, including the autoimmune type 1 diabetes[13–18]. An attractive feature of using gut stem cells to make β-cell mimics is the ease of establishing autologous organoids from biopsies, which can enable mass production and personalized therapies. Aside from the current technical inability to differentiate gut stem cells into functional β-like cells at sufficient efficiency, a significant unknown factor is the documented short lifespans of gut cells in vivo, numbering in days to several weeks[19,20]. This raises the concern as to whether insulin-secreting cells made from human gut tissues will be sufficiently stable and durable as an engraftable therapeutic.

In this study, we developed a robust 3-step protocol to induce cultured hGSCs from multiple donors to differentiate into islet-like organoids at high efficiency, containing approximately 70% β-like cells and other islet-like endocrine populations. GINS organoids exhibited glucose responsiveness 10 days after induction. They were stable upon transplantation for as long as we tracked them (6 months), secreted human insulin and reversed diabetes in mice. No proliferative cells were detected in transplanted GINS organoids whereas hGSCs perished upon engraftment. GINS organoids thus possess favorable attributes as a potential transplantable therapeutic. We further characterized the unique differentiation path leading from hGSCs to GINS organoids with single cell RNA-sequencing (scRNA-seq). This study establishes a promising approach to procuring autologous human insulin producers for diabetes treatment.

Results

Generating islet-like organoids from human stomach samples

Our previous study in mice suggested that stomach tissues are more amenable to adopting β-cell fate than intestinal tissues[10]. We therefore focused on using human gastric stem cells (hGSCs) to generate insulin-secreting cells. The human stomach has three distinct parts: the corpus, pylorus (antrum), and cardia, with corpus mucosa being most abundant. Biopsy samples from all three regions have been grown successfully as organoids in three-dimensional (3D) Matrigel or as 2D flat stem cell colonies, while maintaining their regional

identity in culture[9,21,22]. After in vitro differentiation, hGSCs produce gastric mucosal cells including acid- and mucus-secreting cells[9,21,22]. In this study, we primarily used corpus tissues because of its ready availability.

For the ease of scaling stem cell production, we used 2D culture to expand hGSCs. Each biopsy-sized gastric sample typically yielded 30–40 primary colonies, which can be amplified to $> 10^9$ cells within 2 months (Extended Data Fig. 1a, b). Cultured hGSCs continued to express the stomach stem/progenitor marker SOX9 and the proliferative marker KI67 after many passages (Extended Data Fig. 1a), consistent with prior report[9]. To explore ways to direct hGSCs into functional insulin secretors, we began with the NPM factors (*Ngn3*, *Pdx1,* and *Mafa*). This combination has been shown to confer varying degrees of β-cell properties to non-β cells including pancreatic acinar cells, duct cells, and others[23–27]. However, co-expression of the NPM factors using our previously published polycistronic cassette yielded low insulin expression in cultured hGSCs (Extended Data Fig. 1c). We therefore systematically evaluated conditions that may influence GINS cell formation including the timing of NPM expression, inclusion of additional genetic factors, and medium composition. Several notable observations include: (1) high-level insulin induction required transient NGN3 (for 2 days) followed by stable PDX1 and MAFA expression. This sequence of transgene activation was superior to NPM co-expression or expressing PDX1-MAFA prior to NGN3 (Extended Data Fig. 1d); (2) inclusion of additional β-cell fate regulators such as MAFB or NKX6-1 did not enhance insulin activation (Extended Data Fig. 1e). Critically, we formulated a fully chemically defined serum-free medium for GINS cell differentiation. From a screen of 23 supplements, some of which are employed in the induction of β-like cells from pluripotent stem cells, we found that Nicotinamide and Y-27632 (a ROCK inhibitor) significantly promoted *INS* mRNA levels whereas A8301 (an ALK5 inhibitor) stimulated spontaneous aggregation of nascent GINS cells and expression of several key β-cell transcription factors (Extended Data Fig. 2). The final GINS differentiation medium contained the three supplements, N2, B27, and N-acetyl cysteine in the basal Advanced DMEM/F12 medium.

For inducible NGN3 activation, a *Ngn3* and estrogen receptor (*ER*) fusion gene (*Ngn3ER*) was incorporated into the hGSCs by lentivirus[28]. hGSC differentiation was initiated by 4OH-Tamoxifen treatment of cultured *Ngn3ER*-hGSCs for two days (step 1), followed by lentiviral integration of a *Pdx1-Mafa* co-expression cassette (over 95% infection rate; step 2). Four days later, the nascent GINS cells were aggregated into spherical organoids (step 3), which can persist in the defined medium for up to four weeks (Fig. 1a, b, Extended Data Fig. 3a). Immunohistochemistry of GINS organoids from multiple donors revealed that majority of the organoid cells expressed c-peptide (CPPT, 65.4% ± 5.2%), whereas a minority expressed either glucagon (GCG, 2.2% ± 1.3%), somatostatin (SST, 6.1% ± 2.7%), or ghrelin (GHRL, 4.0% ± 1.5%) (Fig. 1c, d, Extended Data Fig. 3b). The cellular composition of organoids was further evaluated by flow cytometry, with the fractions of CPPT+, SST+ and GCG+ cells largely concordant with the immunostaining data (Fig. 1e). Using a cocktail of SST, GCG and GHRL antibodies, we determined that approximately 92.6% of all CPPT+ cells (or 61.0% of all organoid cells) were mono-hormonal (Extended Data Fig. 3c). The average insulin mRNA levels and insulin content of GINS organoids were comparable to primary islets (Fig. 1f, Extended Data Fig. 3d). GINS organoids from

multiple donors expressed key β-cell markers *ABCC8*, *KCNJ11*, *GCK*, *PAX6*, and *NKX2-2,* at comparable levels to primary islets (Extended Data Fig. 3e).

GINS organoids acquired glucose-stimulated insulin secretion (GSIS) 8–10 days after differentiation (Fig. 2a). In contrast, nascent GINS cells had no or little insulin secretion (Day 7, Fig. 2a). Thus, although a small amount of exogenous insulin was present in culture medium, it was not absorbed in any significant way by the cultured cells and insulin engaged with cell surface receptors has been shown to be shuttled intracellularly for degradation[29]. Notably, glucose responsive organoids could be produced from multiple donors and maintained a batch to batch consistency in functionality (Fig. 2a, Extended Data Fig. 3f). However, the glucose responsiveness of GINS organoids became less consistent after prolonged culture (over 21 days) (Extended data Fig. 3f). GINS organoids responded to repeated glucose challenges as well as the clinical anti-diabetic drug Glibenclamide and the anti-hypoglycemia drug Diazoxide (Fig. 2b, Extended Data Fig. 3g). In dynamic GSIS assays, GINS cells from two separate donors responded robustly to KCl and liraglutide, a GLP-1 analog, but less so to high glucose challenge (Fig. 2c), indicating that they have not attained full functional maturity. Altogether, these data establish a GINS differentiation protocol robust for different donor tissues, yielding glucose-responsive organoids at high efficiency.

GINS organoids contain four endocrine cell types

To better understand the identities of the cells in GINS organoids, we used scRNA-seq to interrogate the transcriptomes of 6,242 organoid cells (Fig. 3a). Clustering with published scRNA transcriptomes of human islets revealed four endocrine cell types that aligned with islet β-, α-, δ-, or ε-cells[30] (Fig. 3a). Clustering with hGSCs and mucus-secreting cells (derived from spontaneous hGSC differentiation in culture) showed almost no gastric cells remaining in GINS organoids (Extended Data Fig. 4a, 4b). The α and δ-like endocrine cells expressed canonical markers of their islet counterparts including *GCG*, *ARX*, *TTR*, and *GC* in α-cells, and *SST* and *HHEX* in δ-cells (Fig. 3b, Extended Data Fig. 4b). GINS cells expressed classical human β-cell markers including *G6PC2, GCK, ABCC8, NKX2-2, PCSK1, PAX6,* and key genes involved in β-cell identity, metabolism, insulin synthesis and secretion, and ion channel activities, but did not express *NKX6-1* (Fig. 3c, Extended Data Fig. 4c). Several genes previously shown to interfere with proper glucose sensing, including *HK1*, *LDHA,* and *SLC16A1*[31], were strongly down-regulated in GINS cells (Extended Data Fig. 4d). GINS organoid cells ceased proliferation after differentiation (Extended Data Fig. 4e). Single-cell transcriptomes of antral GINS organoids also revealed a dominant fraction of β-like cells. No significant numbers of α- and ε-like cells were detected whereas an additional gastrin-expressing cell population was present in antral organoids (Extended Data Fig. 5a–e). Antral organoids exhibited robust GSIS in vitro (Extended Data Fig. 5f).

To further assess the identity of GINS cells, we applied molecular score cards of β-cells (1,034 β-cell-specific genes) and gastric cells (868 stomach-specific genes) benchmarked from published human scRNA data[32,33]. GINS cells scored similarly to islet β-cells in both categories, although there is a residual gastric signature in GINS cells (Fig. 3d). In comparison, hGSCs and mucus-secreting cells possessed low β- and high gastric scores

(Fig. 3d). These data indicate that GINS cells possess the general molecular identity of islet β-cells at the single-cell level, consistent with their glucose responsiveness. Nevertheless, Gene Ontology analysis suggests that GINS cells have lower ribonucleoprotein biogenesis activity than islet β-cells (Extended Data Fig. 6), possibly underlying the functional immaturity of GINS cells in vitro.

GINS cells persist after engraftment and reverse diabetes

In order to evaluate the longevity and functionality of GINS cells in vivo, we transplanted GINS cells under the kidney capsule of immune-compromised NSG mice (0.8 million cells per mouse). We examined the grafts at 2, 4, and 6 months. At each time point, the grafts contained abundant INS+ cells perfused with CD31+ vasculature and minor populations of GCG+, SST+, and GHRL+ cells (Fig. 4a, Extended Data Fig. 7a). Grafted GINS cells expressed PAX6, NKX2-2, PCSK1, and the adult β-cell marker ENTPD3 (also known as NTPDase3)[34] (Fig. 4a). Electron microscopy showed that the electron-dense granules of the GINS cells were not fully condensed (Extended Data Fig. 7b), likely reflecting lower levels of SLC30A8 (Extended Data Fig. 7c), the activity of which is required for the granule morphology[35]. Loss of SLC30A8 is associated with protection against type 2 diabetes[36,37].

The majority of the GINS grafts showed glucose-stimulated insulin secretion (Fig. 4b). Accordingly, transplantation of 6–8 million GINS cells from donor #6 into NSG mice rendered diabetic by streptozotocin (STZ) rapidly suppressed hyperglycemia and maintained glucose homeostasis for over 100 days, until removal of the grafts by nephrectomy (Fig. 4c, Extended data Fig. 7d). A second cohort of mice transplanted with organoids from a different donor (# 10, 6 million cells per mouse) yielded similar results although the glycemic control was less tight (Fig. 4c). Glucose tolerance improved significantly in both engrafted groups (Fig. 4d). Importantly, we detected no proliferating cells within the grafts at any time point (Fig. 4e). To directly evaluate the fate of hGSCs upon transplantation, we engrafted 0.5 million undifferentiated mCherry-labeled hGSCs under the kidney capsule of 6 NSG mice. After 80 days, no surviving cells were detected at the graft sites (Extended Data Fig. 7e), consistent with the well-documented reliance of hGSCs on high WNT signaling to survive[38,39]. We conclude that GINS cells, derived from human gut stem cells, can be long-lived and functional and pose little risk of uncontrolled proliferation after transplantation.

Comparison of GINS single-cell transcriptomes before and after transplantation (6,242 cells in vitro, 3,502 cells in vivo at 3 months post transplantation) showed molecular changes consistent with maturation, including enhanced expression of *NKX2-2, PAX6, UCN3,* and *ENTPD3* and reduced *TFF2* and *GHRL* (Fig. 3f). Key ribonucleoproteins were up-regulated whereas several pathways elevated in cultured GINS cells were down-regulated after transplantation (Extended Data Fig. 7f–h). Insulin expression, while variable in cultured GINS cells, became notably more uniform in the grafted cells (Fig. 4f). Correlation coefficient analysis based on the top 2,000 variable genes showed that GINS transcriptomes became more homogeneous after transplantation, a characteristic shared with islet β cells (Fig. 4g). These results together indicate molecular maturation of GINS cells after transplantation.

Developmental trajectory of GINS cells

hGSCs normally produce stomach-specific cells including mucus- and acid-secreting cells. To understand how their differentiation path is rerouted in GINS formation, we used scRNA-seq to sample key stages in GINS derivation and reconstructed the developmental trajectory with pseudotime ordering. In total, 9,544 high-quality single cell transcriptomes were collected from four samples: hGSCs, endocrine progenitors (2 days after NGN3 activation), GINS precursors (4 days after PDX1-MAFA expression), and GINS organoids (14 days after aggregation) (Fig. 5a). Clustering analysis showed one stem cell ($SOX9^{High}TFF2^{High}LGR5^{High}$), two endocrine progenitors ($SOX4^{High}CHGA^{Low}$ and $SOX4^{High}CHGA^{High}$), one GINS precursor ($GAL^{High}SSTR2^{High}$), and four endocrine cell populations (Fig. 5b, c, Extended Data Fig. 8a) along pseudotemporal progression (Fig. 5d, Extended Data Fig. 8b). Notably, somatostatin-expressing δ-like cells emerged ahead of the other endocrine cells (Fig. 5a, 5b, 5d). *Pdx1* and *Mafa* transgene expression was significantly higher in GINS cells than the other endocrine cells, suggesting higher transgenes promoted β-cell fate at the expense of the other endocrine cell types (Fig. 5e). Gene Ontology analysis showed rapid down-regulation of stem cell and proliferative pathways upon endocrine differentiation (Fig. 5f). WNT and NOTCH signaling were active in endocrine precursors whereas histone modification was associated with the GINS precursors. Functional pathways characteristic of β-cells such as hormone transport and secretion, and mitochondria and ribosome activities, emerged last (Fig. 5f).

Waves of transcription factor (TF) activations accompanied the progression from hGSCs to GINS cells, likely orchestrating the stepwise acquisition of GINS fate (Extended Data Fig. 8c). Regulon analysis showed active ASCL1 and SOX4 regulons in endocrine progenitors (Extended Data Fig. 9a, 9b). Early-activating GINS regulons included ones for HHEX, PAX4, and ISL1, while late-activating regulons included ones for RFX6, PAX6, PDX1 and MAFB (Extended Data Fig. 9a, 9b).

Pseudotime ordering and RNA velocity analysis suggest that β-like cells descended from GINS precursors (Fig. 5d, Extended Data Fig. 9c), which expressed several markers including *SSTR2* and *GALANIN* (GAL), a neuropeptide predominantly expressed in the nervous system (Fig. 6a). To evaluate whether GAL+ precursors can give rise to CPPT+ cells, we made a reporter construct in which GFP expression was driven by human *GAL* promoter and integrated this construct into a hGSC line (Fig. 6b). Six days post differentiation, GFP expression was activated, consistent with the appearance of GINS precursors at this stage. We then purified the GFP^high cell fraction by flow cytometry and aggregated the cells into organoids. After overnight culture, the nascent GINS organoids contained predominant GAL+ cells (89.9% ± 3.0%) whereas a small fraction (14.2% ± 5.9%) had barely detectable levels of CPPT (Fig. 6c–e). After 14 days of culture, the percentage of GAL+ cells and the average GAL staining intensity decreased while the percentage of CPPT+ cells rose to 61.2% ± 7.5% and CPPT staining intensity significantly increased (Fig. 6c–e). These data show that GAL+ cells can indeed serve as precursors to CPPT+ GINS cells. We note that GALANIN is expressed in human islets, including some β-cells (Fig. 6f). Upon transplantation and maturation, *GAL* expression in GINS cells further decreased (Fig. 6g). Altogether, our data support a model in which sequential

Ngn3 and Pdx1-Mafa expression triggered waves of TF activations that led gut cells onto a distinctive differentiation path, including a galanin-expressing precursor, before adopting GINS identity (Fig. 6h).

Discussion

In this study, we describe a robust protocol to derive insulin-secreting organoids from cultured hGSCs with high efficiency. The glucose-responsive GINS cells became long-lived insulin secretors and restored glucose homeostasis in diabetic mice. Some of the attractive features of using gastric stem cells to make β-cell mimics include: the relative ease of obtaining gastric biopsies via endoscopy to enable production of autologous grafts; GINS organoid generation involves a relatively straightforward 3-step protocol; GINS organoids gain a measure of functionality relatively quickly, at 10 days post induction; GINS organoids pose little tumorigenic risks; the same protocol works well on hGSCs from different donors; and lastly, GINS organoids persist for many months after transplantation.

The leading strategy of producing islet-like organoids today is differentiation from human embryonic stem cells, yielding sc-islets[40]. An autologous approach using induced pluripotent stem cells (iPSCs) is feasible but faces significant hurdles[18], one of which is the lengthy process in generating iPSCs. The hGSC approach saves time and effort by directly obtaining patient stem cells and producing organoids with a simpler differentiation protocol, thus offering a useful alternative to iPSCs.

In addition to the autologous approach, more than 250,000 bariatric surgeries, in which a large portion of the gastric corpus is removed, are performed yearly in the United States alone. These discarded tissues could support the building of gastric stem cell biobanks, enabling major histocompatibility complex (MHC) matching to find suitable donors for transplantation. For treatment of type 1 diabetes, recent advances in engineering immune-evasive organoids could guide the generation of GINS organoids that survive an autoimmune environment[41–43].

GINS grafts, unlike sc-islet grafts, lack a significant number of α- and δ-like cells. These endocrine populations have been suggested to fine-tune glucose responsiveness of β-cells[44]. The long-term consequence of this particular composition of GINS grafts requires further study and if necessary, a new method should be developed to boost the number of α- and δ-like cells.

Our data uncovered significant differences between mouse and human gastric tissues in their response to the inducing NPM factors. Whereas mouse corpus stomach resisted NPM induction[9], human corpus cells were amenable. And while simultaneous expression of NPM factors induced abundant β-like cells from mouse antral EECs in situ[9], it induced few from cultured human antrum and corpus stem cells. The molecular basis for these species-specific effects remains to be determined.

Although GINS cells resemble cadaveric β-cells, there are notable differences, including the retainment of a residual gastric molecular signature in GINS organoids. We formulated a fully chemically defined serum-free medium for GINS organoid differentiation, but the

organoids did not attain full functionality in vitro and after prolonged culture, their glucose-responsiveness waned. Developing a new medium to promote organoid maturation in vitro will be a priority of future studies. Additional optimizations are also needed to move the GINS technology toward clinics, including replacement of lentivirus with a safer gene activation method.

Methods

Lentivirus packaging and titration.

The lentiviruses were packaged using Lipofectamine 3000 (Thermo Fisher Scientific, L3000001) as previously described[45]. Viral supernatant was cleared by centrifugation followed by filtration using a 0.45 μm polyethersulfone (PES) filter. Viruses were then concentrated 20-fold by Centrifugal Filter (Millipore Sigma, UFC910024). Concentrated viruses were aliquoted and stored at –80°C. To measure the titer of lentiviruses, HEK293FT (ThermoFisher, R70007) cells were seeded in 24-well plates to be ~90% confluent at infection. Virus was diluted in DMEM medium containing 10% FBS and 10 μg/mL polybrene and added to the cells. Forty-eight hours post infection, the number of fluorescence-positive cells was counted under a fluorescence microscope if the lentiviral vector carried a fluorescence marker (e.g., mCherry for Lenti-EF1a-*Ngn3ER-Puro^R-mCherry*). Otherwise, transduced cells were visualized by an immunofluorescence assay (e.g., MAFA staining for Lenti-TetO-PM or Lenti-CMV-PM). Viral titers were defined by the transduction units per mL (TU/mL).

Human samples.

We used one biopsy sample (Donor-CH) from Boston Children's Hospital under the protocol (IRB-P00000529). All studies involving human samples were approved by ethics committees at Boston Children's Hospital and Weill Cornell Medical College. The autopsy samples were from either the International Institute for the Advancement of Medicine (IIAM) or The National Disease Research Interchange (NDRI). Informed consent was obtained from the participants and or parents/guardian for these studies. Subject details are described in Supplementary Table 1. Human islets were obtained from Prodo Labs.

Derivation and culture of human gastric stem cells from primary mucosal tissues.

Primary human gastric stem cells were isolated as described in detail[46]. Human gastric samples (3–5 mm in size) were vigorously washed with cold DPBS 3 times and cut into smaller pieces with a sharp scalpel. Tissue was then incubated with F12K medium containing 2 mg/ml collagenase type IV (Worthington, LS004188) at 37°C with pipetting every 5–10 min until most of the glandular cells were released and appeared in solution as clusters. Cells were neutralized with F12K supplemented with 10% FBS and centrifuged at 500 x g for 5 min. Pelleted cells were resuspended in human gastric stem cell culture medium (hGSC medium) and seeded on mitomycin-C-inactivated mouse embryonic fibroblasts (MEF, E13.5-14.5, DR4 strain, The Jackson Laboratory, 003208) coated 3-cm dish.

The hGSC medium was formulated using a method slightly modified from a published report[9]: basal medium composed of 66.7% DMEM (high glucose, Thermo Fisher Scientific, 11–965–118) and 33.3% F12K (Thermo Fisher Scientific, 21127030) was supplemented with 18% FBS (R&D systems, S11150), 10% R-Spondin-2 conditioned medium, 10 mM Nicotinamide (Sigma-Aldrich, N5535), 25 μM Primocin (Invivogen, ant-pm-1), 1 μM A8301 (Cayman, 9001799), 5 μg/mL insulin (Sigma-Aldrich, I0516-5ML), 10 μM Y-27632 (LC Laboratories, Y-5301), 1 μM DMH1 (Cayman, 16679), 50 ng/mL EGF (R&D Systems, 236-EG-01M), and 2 μM T3 (Sigma-Aldrich, T6397).

hGSCs were maintained at 37 °C in a 7.5% CO_2 incubator. Culture medium was changed every 2–3 days. Y-27632 was withdrawn 24 h post passage. hGSC colonies were split every 4–6 days at a ratio between 1:3 and 1:5 as follows: cells were washed twice with DPBS and dissociated by 10–12 min incubation in TrypLE (Thermo Fisher Scientific, 12604021) with pipetting at the end. Cells were then neutralized by DMEM medium with 10% FBS and centrifuged at 300 x g for 5 min. Pelleted cells were resuspended in hGSC medium and then seeded on an inactivated-MEF-coated dish.

hGSCs engineering with Lentiviral infection for transgene and reporter gene expression.

Human gastric stem cells were engineered as described in detail[46]. To engineer hGSCs, cells were passaged in one well of 6-well plate 24 hours prior to lentiviral transduction. Cells were washed with DPBS and overlaid with hGSC medium containing 10 μg/mL polybrene and 25 μL of lentivirus (viral titer: ~10^8 TU/mL). Spinfection was then performed as follows: the cell culture with lentivirus was spun at 1000 x g for 30 min at 37°C and then incubated at 37°C in a 7.5% CO_2 incubator for 48 hours. The medium was changed to hGSC medium containing 1 μg/mL puromycin or 10 μg/mL Blasticidin according to the selection marker incorporated into the construct for 2 weeks. The *Ngn3ER*-hGSCs were labeled with constitutive mCherry expression by incorporation of a polycistronic cassette EF1α-*Ngn3ER*-*Puro^R*-*mCherry* (*Puro^R*, puromycin resistant gene). To establish the Ngn3 and Pdx1-Mafa dual inducible cell line (*Ngn3ER*/TetO*PM*-hGSCs), *Ngn3ER*-hGSCs were infected by Lenti-TetO-PM (lentivirus carrying the polycistronic cassette TetO-*Pdx1-Mafa*) *and* PGK-*rtTA-Blast^R* (*Blast^R*, blasticidin resistant gene). To establish the pGAL-*GFP* reporter cell line (*Ngn3ER*/pGAL-*GFP*-hGSCs), *Ngn3ER*-hGSCs were infected by lentivirus carrying transgenic *GAL* promoter (1,591 bp, upstream region of the TSS (transcription start site)) driven GFP reporter (pGAL-*GFP*) and PGK-*Blast^R*. Doxycycline (Dox, 1 μg/mL) or 4-OH-Tam (1 μM, Sigma-Aldrich, H7904) were added to the medium to induce the expression of TetO-driven transcription or Ngn3ER activation.

Supplement screen to formulate chemically defined serum-free medium for GINS differentiation.

Ngn3ER/*PM*-hGSCs were seeded 5 days prior to differentiation in 96-well plate. To start differentiation, 1 μM 4-OH-TAM was added and incubated for 2 days. The culture medium was then changed to serum-free basal medium with one supplement and Doxycycline to activate *Pdx1-Mafa* expression. The basal serum-free medium for screens was prepared as follows: advanced DMEM/F12 (Thermo Fisher Scientific, 12634010) was supplemented with 10 mM HEPES (Thermo Fisher Scientific, 15–630–080), 1X GlutaMAX (Thermo

Fisher Scientific, 35050061), 1X B-27 (Themo Fisher Scientific, 17504044), 1X N-2 (Thermo Fisher Scientific, 17502048), 25 μM Primocin, and 500 μM N-Acetyl-L-Cysteine (NAC) (Sigma-Aldrich, A9165). Seven days after supplement treatment, we assessed (1) spontaneous clustering of nascent GINS cells by live imaging of mCherry⁺ cells, and (2) qPCR of *INS* mRNA levels. We then analyzed multiple β-cell markers with qPCR on samples treated with Nicotinamide, Y-27632 and A8301.

Generation of GINS organoids (Supplementary Table 2).

GINS organoids were generated as described in detail[46]. Plasmids are available from Addgene under a uniform biological material transfer agreement. The procedure is briefly summarized as follow:

1. Ngn3ER activation (Differentiation to endocrine progenitors) (day 0–2): *Ngn3ER*-hGSCs were seeded 4–5 days prior to differentiation. Cells were washed with DPBS and overlaid with hGSC medium containing 1 μM 4-OH-TAM.

2. Pdx1-Mafa transduction (Differentiation to GINS precursors) (day 2–6): Endocrine progenitors were gently washed with DPBS, incubated in DPBS for 5–10 min, and detached by pipetting. Pelleted cells were then digested in TrypLE at 37°C for 10 min with pipetting every 3–5 min. Dissociated endocrine progenitors were transduced by Lenti-CMV-PM (lentivirus carrying the polycistronic cassette CMV-*Pdx1-Mafa*) at an MOI of 10 by spinfection in medium composed of 50% of hGSC medium, 50% of GINS medium, and 10 μg/mL polybrene. Cells were then transferred to tissue culture dishes (~10^7 cells per 10-cm dish) coated with Fibronectin (1:50, Sigma-Aldrich, F4759) and Matrigel (1:50, VWR, 47743–722). On day 4, the culture medium was changed to medium consisting of 75% GINS medium and 25% hGSC medium.

3. GINS organoid formation (day 6–21): GINS precursors were dissociated by 5–10 min TrypLE treatment and aggregated (typically 2.0–2.4 million cells/well) in AggreWell400 (STEMCELL Technologies, 34450) using the manufacturer's recommended protocol. Medium was changed every 2–3 days. Aggregates normally formed within 24 hours.

4. GINS medium for this study was formulated as the follows: advanced DMEM/F12 supplemented with 10 mM HEPES, 1X GlutaMAX, 25 μM Primocin, 500 μM NAC, 1X B-27, 1X N-2, 10 mM Nicotinamide, 1 μM A8301, and 10 μM Y-27632.

Alternatively, the dual inducible cell line *Ngn3ER*/TetO*PM*-hGSCs was used for differentiation optimization. Instead of lentiviral transduction at step (2), 1 μg/mL Dox was added to the medium starting on day 2 to induce expression of Pdx1-Mafa.

Static glucose-stimulated insulin secretion (GSIS).

Ten to twenty GINS organoids were sampled for each group. Organoids were washed with RPMI-1640 no nutrient medium (RPMIN, MyBioSource, MBS652918), and equilibrated in 3.3 mM glucose RPMIN for 2 hours. Organoids were incubated in low-glucose RPMIN

for 1 hour, and supernatant was collected. Organoids were then incubated in high-glucose RPMIN for 1 hour, and supernatant was collected. For sequential glucose challenge, organoids were washed 2 times in RPMIN prior to the next stimulation. Secreted insulin was measured using the Stellux Chemi Human Insulin ELISA (ALPCO Diagnostics, 80-INSHU-CH10).

Dynamic GSIS with perifusion.

Twenty GINS organoids were sampled for each group. Organoids were washed with RPMIN and equilibrated in 1 mM glucose RPMIN for 2 hours at 37°C incubator. The assay was performed in RPMIN on a temperature-controlled (37°C) perifusion system (Biorep Technologies). Organoids were loaded in chambers and perifused at a flow rate of 100 μL/min in the following steps: (1) 48 min in 1 mM glucose, (2) 24 min in 2 mM glucose, (3) 36 min in 20 mM glucose, (4) 24 min in 20 mM glucose with 100 ng/mL Liraglutide (Cayman, 24727), (5) 48 min in 2 mM glucose, (6) 20 min in 2 mM glucose with 30 mM KCl. Secreted insulin was measured using the Stellux Chemi Human Insulin ELISA.

Transplantation studies in normoglycemic and hyperglycemic mice.

All mouse experiments were conducted under the IACUC protocol 2018–0050 at Weill Cornell Medical College (WCMC). Mice were housed in a temperature- and humidity-controlled environment with 12 hours light/dark cycle and food/water ad libitum. Mice were fed with chow diet (PicoLab Rodent Diet 5053). NSG mouse breeders were purchase from the Jackson Laboratory (Strain #:005557). NSG breeding was conducted in WCMC. Transplantations were performed with 8–12 weeks old male NSG mice. GINS organoids or human islets were transplanted under the capsule of the left kidney in NSG mice anesthetized with isoflurane. For glucose tolerance test, transplanted mice were fasted for 6 hours and injected with 2 g/kg glucose intraperitoneally. Blood glucose was then measured at indicated time points by glucometer. For in vivo GSIS, transplanted mice were fasted overnight and injected with 2 g/kg glucose intraperitoneally. Blood before injection and 1 hour post glucose injection was collected by submandibular bleeding with Microvette 300 capillary blood collection tube (Sarstedt, 20.1309.100). Serum was separated from the blood for insulin measurement by Stellux Chemi Human Insulin ELISA. For the diabetes rescue experiment, male mice were injected with four doses of Streptozotocin (35 mg/kg/d) on four consecutive days to induce hyperglycemia. Mice that showed hyperglycemia (>250 mg/dl) on four consecutive days were selected for transplantation. Sham transplantation was conducted by operating the surgical procedure without infusing cells. Random fed blood glucose was monitored 2 times per week. To remove grafts, a survival nephrectomy was performed after 90–100 days post transplantation. Briefly, the left kidney was ligated at the renal hilum using 3–0 silk and then resected.

Immunofluorescence.

GINS organoids were fixed in 4% PFA for 15 min at room temperature. Kidney samples were fixed in 4% PFA at 4°C for 1 hour. Samples were washed in PBS, incubated in PBS containing 30% sucrose overnight. Samples were frozen in OCT (Tissue-Tek) next day, and then cryo-sectioned. Following PBS wash, sections were blocked for 1 hour at room temperature in blocking buffer: 10% normal donkey serum (Jackson ImmunoResearch,

017–000–121) in PBST (0.1% TritonX-100 in PBS). Sections were then incubated with primary antibodies in blocking buffer overnight at 4°C. The following primary antibodies were used in this study: at anti-C-peptide (DHSB; GN-ID4; 1:300), rabbit anti-somatostatin (Dako; A0566, 1:500), goat anti-ghrelin (Santa Cruz, sc-10368, 1:400), guinea pig anti-glucagon (Linco, 4031-01F, 1: 2000), rabbit anti-MAFA (Bethyl; A700-067; 1:1000), guinea pig anti-insulin (Dako; A0564; 1:2000), rat anti-CD31 (BD, 550274, 1:50), mouse anti-ENTPD3 (NTPDase3) (developed in house, available at ectonucleotidases-ab.com, 1:1000), rabbit anti-PAX6 (Millipore; AB2237, 1:1000), mouse anti-NKX2-2 (DSHB; 74.5A5-s, 1:25), rabbit anti-PCSK1 (Millipore, AB10553, 1:500), mouse anti-GAL (Santa Cruz, sc-166431, 1:2000), rabbit anti-SOX9 (Santa Cruz, sc-20095, 1:50), mouse anti-KI67 (BD, 556003, 1:500). Slides were washed three times in PBST, followed by secondary antibody incubation in blocking buffer with DAPI for 1 hour at room temperature (protected from light). Following 3 washes in PBST, slides were mounted in mounting medium (Vector Laboratories, H-1700-10) and covered with coverslips. The representative images were captured using either a confocal microscope (710 Meta) or a Nikon fluorescence microscope. Images were processed by Zen (3.4 blue edition) or ImageJ (1.53t).

RNA extraction, reverse transcription, and real-time PCR.

RNA was extracted (Qiagen, 74034) and reversely transcribed (Thermo Fisher Scientific, 43–688–13) to complementary DNA (cDNA). cDNA was diluted and then quantified by real-time PCR with TaqMan assay listed in Supplementary Table 3. For optimization experiments, Cells-to-Ct Kit was used (Thermo Fisher Scientific, A35377).

Fluorescence-activated Cell Sorting (FACS).

For quantitative flow cytometry, GINS organoids were dissociated in TrypLE for 40 min. Dissociated cells were stained with Fixable Viability Dye 455UV (Thermo Scientific, 65–0868–14) according to the manufacturer's manual. Cells were then fixed and permeabilized using Intracellular Fixation & Permeabilization Buffer Set (Thermo Scientific, 88–8824–00) according to the manufacturer's manual. Fixed cells were then incubated in 1X permeabilization buffer with primary antibodies for 1 h at room temperature and washed with permeabilization buffer for 3 times and resuspended in flow cytometry staining buffer (Thermo Scientific, 00–4222). Stained cells were then passed through a 40 μm nylon strainer before being sorted (Supplementary Fig. 1). The following primary antibodies were used in this study: mouse anti-C-peptide Alexa Fluor® 647 (BD, 565831, 1:25), mouse anti-glucagon Alexa Fluor® 488 (R&D, IC1249G, 1:25), mouse anti-somatostatin Alexa Fluor® 488 (BD, 566032, 1:25).

For live cells sorting, cells were dissociated in TrypLE (40 min for hGSCs, 5 min for endocrine progenitors, 5 min for GINS precursors and 40 min for GINS organoids), and pelleted. Cells pellet was resuspended in FACS buffer (1% glucose, 10 mM HEPES, 10 μM Y-27632, 1 mM N-acetyl-l- cysteine, and 2% FBS in DPBS) and passed through a 40 μm nylon strainer before being sorted (Supplementary Fig. 2–4).

To purify GAL-GFP+ cells, Ngn3ER/pGAL-GFP-hGSCs were seeded and differentiated toward GINS cells. On day 7 post differentiation, cells were sorted for GFP+ cells. Sorted

cells were then aggregated into organoids and analyzed 1 and 14 days post aggregation. FACS data was analyzed by FACS DIVA 8.0.1 or FCS Express 7 (7.16.0035).

Single cell RNA-seq (scRNA-seq) from cultured and transplanted GINS organoids and multiplex scRNA-seq.

For the time-course study of GINS generation, samples at different time points were harvested on the same day from parallel cultures. Cells were dissociated in TrypLE. FACS sorting was conducted to purify mCherry+ DAPI− cells. Purified samples were then multiplexed according to the 10X genomics protocol CG000391. Briefly, 2×10^5 sorted cells from each time point were washed in PBS with 0.04% BSA (Millipore Sigma, A1595), and then labeled with multiplexing oligo individually for 5 min at room temperature. Following two washes in PBS with 1% BSA, equal number of labeled cells from different time points were then pooled. In total 30,000 cells were then loaded for 10X genomics. To compare corpus and antral GINS organoids, cells were dissociated by TrypLE on day 21 post induction. To harvest GINS cells from the grafts, the grafts under the kidney capsule were removed with a scalpel and minced. The tissues were digested with type III collagenase (300U/ml in RPMI 1640) for 1 hour, followed by 5–10 min TrypLE treatment with pipetting. Digested tissue was filtered through 40 μm nylon strains and purified by FACS with mCherry+ and DAPI− gating. Samples were kept in GINS medium on ice until ready to be processed by 10X genomics single-cell droplet sample preparation workflow at the Genomics Core Facility at Weill Cornell Medicine as previously described[47].

scRNA-seq analysis.

1. <u>Demultiplexing and reads alignment</u>: Human islets (donor #1, #2, #3, #4 and #9) scRNA-seq datasets were downloaded from Gene Expression Omnibus (GEO) database (GSE114297)[30]. Multiplexed sequencing data from the Illumina NovaSeq6000 were demultiplexed using the 'multi' pipeline from Cell Ranger (v6.1.2). Each of the four Cell Multiplex Oligo labels was assigned a unique sample ID. All the datasets were then processed with the 10X built mouse and human reference 'refdata-gex-GRCh38-and-mm10-2020-A'z'.

2. <u>Quality control and count normalization</u>: Cell Ranger outputs were used as input to create Seurat objects by Seurat (v4.1.1)[48]. Cells that express more murine genes than human genes were defined as contaminant murine cells (e.g., murine host cells from kidney) and removed from the datasets. Murine features were then removed. Low-quality cells were removed as follows: In general, cells were considered low-quality if the number of detectable genes or read counts is below the 3rd percentile or above the 97th percentile of the datasets, or percentage of mitochondrial genes is more than 18. *NormalizeData* function was used for normalization with default parameters. Putative doublet cells were identified by DoubletFinder (2.0.3) and removed[49]. SoupX (1.6.1) was used to remove ambient RNA in the human islet datasets[50].

3. <u>Scaling, dimension reduction, cell clustering, differential expression analysis and cell annotation</u>: The normalized data was scaled by *ScaleData* function with mitochondrial genes percentage regressed out. Cell cycle status was inferred

by *CellCycleScoring* function and regressed out for the time course study. Principal component analysis (PCA) was performed on the scaled data by *runPCA*. To place similar cells together in 2-dimensional space, selected top principal components (PCs) of human islet, GINS organoid (corpus), antral GINS organoid, GINS generation time course and GINS graft (corpus) were used as input respectively in non-linear dimensional reduction techniques including tSNE and UMAP. The same PCs of each sample were used to construct K-nearest neighbor (KNN) graph by *FindNeighbors* function. To cluster cells, *FindClusters* function was used with a range of resolution between 0.2 to 2. Cells clustered by different resolutions were all visualized by *DimPlot* function. To identify markers of each cell cluster, *FindAllMarkers* function was implemented using the following parameters: only.pos = TRUE, min.pct = 0.3, logfc.threshold = 0.3. Human islets cells were firstly automatically annotated by the R package SingleR (1.10.0) with a publish islets dataset as reference[32]. The annotation of the islet dataset was then slightly modified according to the clustering results and cluster markers. Non-endocrine cells or unclear cell types were removed from the human islet dataset. All the other datasets were annotated manually according to markers and integration results.

4. <u>Integration analysis</u>: GINS organoids (corpus) were integrated with antral GINS organoids, human islets endocrine cells, and GINS grafted cells respectively. The genes that were used for integration were chosen by *SelectIntegrationFeatures* function with default parameter. Integration anchors were identified by *FindIntegrationAnchors* function and used to integrate two datasets together with *IntegrateData* function. All the integrated datasets were scaled with mitochondrial genes regressed out. Dimensions were reduced by PCA, tSNE and UMAP.

5. <u>Identity scoring</u>: Signature gene sets (Supplementary Table 4) were downloaded from cell type signature gene sets (C8 collection) of Molecular Signature Database (v7.5.1). Specifically, the gastric signature is a gene list containing curated cluster markers for gastric chief, immature pit, mature pit, isthmus, neck, and parietal cells identified in the study[33], while the signature of β-cell is the MURARO_PANCREAS_BETA_CELL gene set[32]. Both gene sets were then applied as inputs in the *AddModuleScore* function of Seurat with default parameters, which calculates module scores for feature expression programs on single-cell level.

6. <u>Pseudotime trajectory, RNA velocity, regulon and Gene Oncology (GO) analysis</u>: Seurat object of the time course dataset was converted to monocle 2 (2.24.0) CellDataSet object[51–53]. Size factor and dispersion were estimated by *estimateSizeFactors* and *estimateDispersions* function respectively. Cell type markers identified by Seurat were sorted based on adjusted p-value. Top 100 markers of each cell type were marked by *setOrderingFilter* function for later trajectory construction. Data dimension was then reduced by *reduceDimsion* function with the following arguments: max_components = 2, method = 'DDRTree'). Cells were then ordered along the trajectory by *orderCells* function.

To build pseudotime trajectory on UMAP, Seurat object was converted to monocle 3 (1.2.9) object by *as.cell_data_set* function. Cells were then clustered by *cluster_cells* function. The trajectory of GINS precursor, δ-like, β-like and α-like cells, which were in the same partition, was constructed by *learn_graph* followed by *order_cells* function. RNA velocity was evaluated by *RunVelocity* function provided by R packages velocyto.R (0.6) and SeuratWrappers (0.3.0)[54]. Regulon activity was computed by SCENIC (1.3.1) R package as previously described[55]. GO analysis was done by *enrichGO* function in ClusterProfiler (4.4.4) as previously described[56,57].

Statistics and reproducibility.

Statistical analysis and figure plotting were done using GraphPad Prism 9 or R (4.2.2). P values are provided in the figures. Sample size, and statistical methods are described in figure legends. Data are presented as the mean ± s.d. or s.e.m. as indicated. All experiments were repeated as indicated; n indicates the numbers of independent repeats as indicated. Male mice of similar age were used for transplantation and randomly assigned to experimental groups. No statistical methods were used to pre-determine sample sizes but our sample sizes are similar to those reported in previous publications[58,59]. Data distribution was assumed to be normal but this was not formally tested. Single cells with poor quality sequencing data were excluded as described. For transplantation experiments with diabetic mice, mice that did not develop hyperglycemia after STZ treatment were not used. Data collection and analysis were not performed blind to the conditions of the experiments.

Extended Data
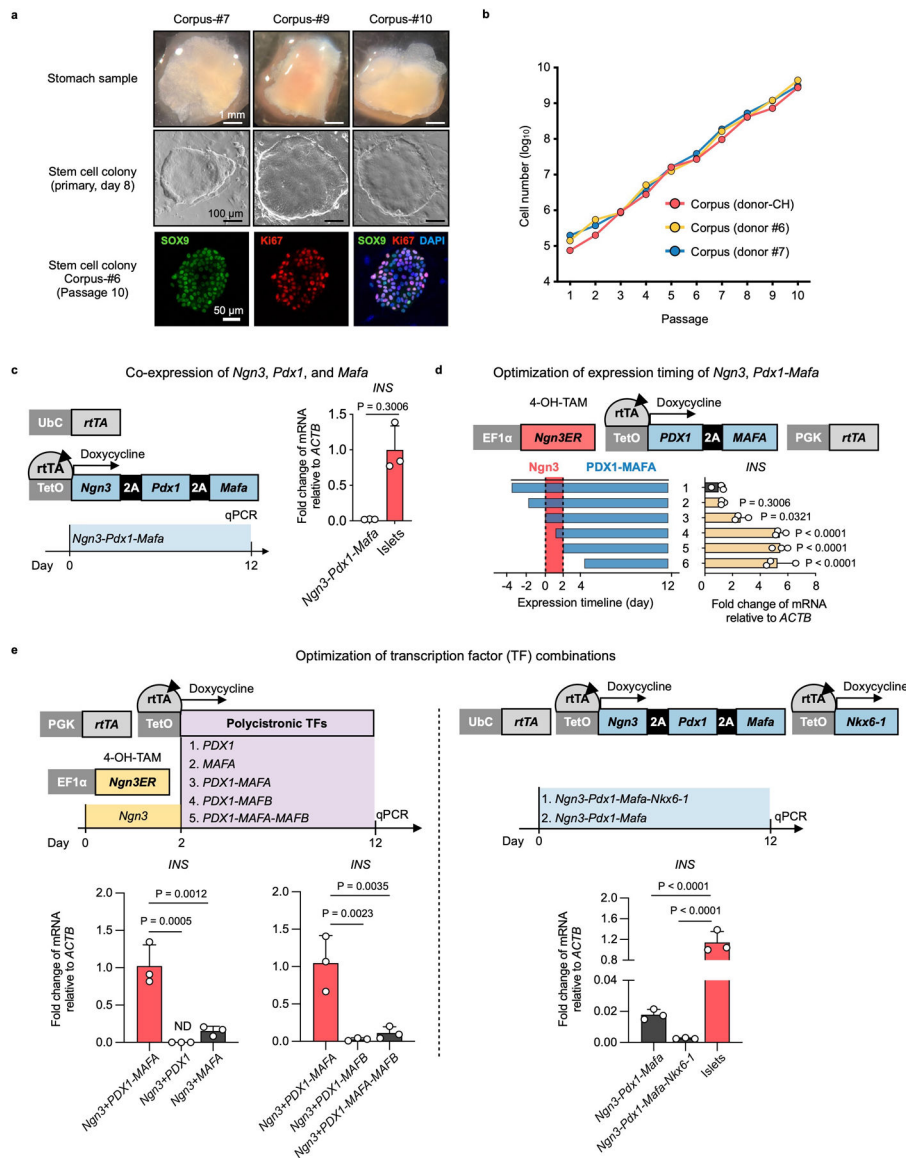
Extended Data Fig. 1 |. Optimizing conditions to induce insulin-expressing cells from cultured human gastric stem cells.

a, Top: stomach samples from 3 different donors; middle, primary hGSC colonies derived from the stomach samples; bottom, immunofluorescence of passage-10 hGSC colony staining for SOX9 and KI67. **b**, Growth kinetics of hGSCs from three different donors. **c**, Co-expression of *Ngn3*, *Pdx1*, and *Mafa* using a polycistronic inducible construct in hGSCs yielded low levels of insulin expression (n=3 biological independent samples). Ubc: ubiquitin promoter. **d**, To optimize the relative timing of Ngn3 and Pdx1- MafA expression, we expressed a Ngn3ER fusion protein in which Ngn3 activity was induced by 4-OH Tamoxifen (4-OH-TAM). Polycistronic PDX1 and MAFA co-expression was controlled by rtTA-TetO and activated by the addition of Doxycycline in the culture medium. Higher *INS* expression was achieved by sequential activation of the transcription factors NGN3

and PDX1-MAFA. n=3 independent experiments. **e**, Comparison of PDX1-MAFA with the other transcription factor combinations in insulin induction. 2- day Ngn3ER induction (by 4-OH-TAM) preceded the other TFs, or alternatively, co-expression cassettes were used. ND: not detected. n=3 independent experiments. **c**, **d**, **e**, Data presented as mean ± s.d.; two-tailed unpaired t-test (**c**), or one-way ANOVA with Dunnett multiple comparisons test (**d**, **e**).
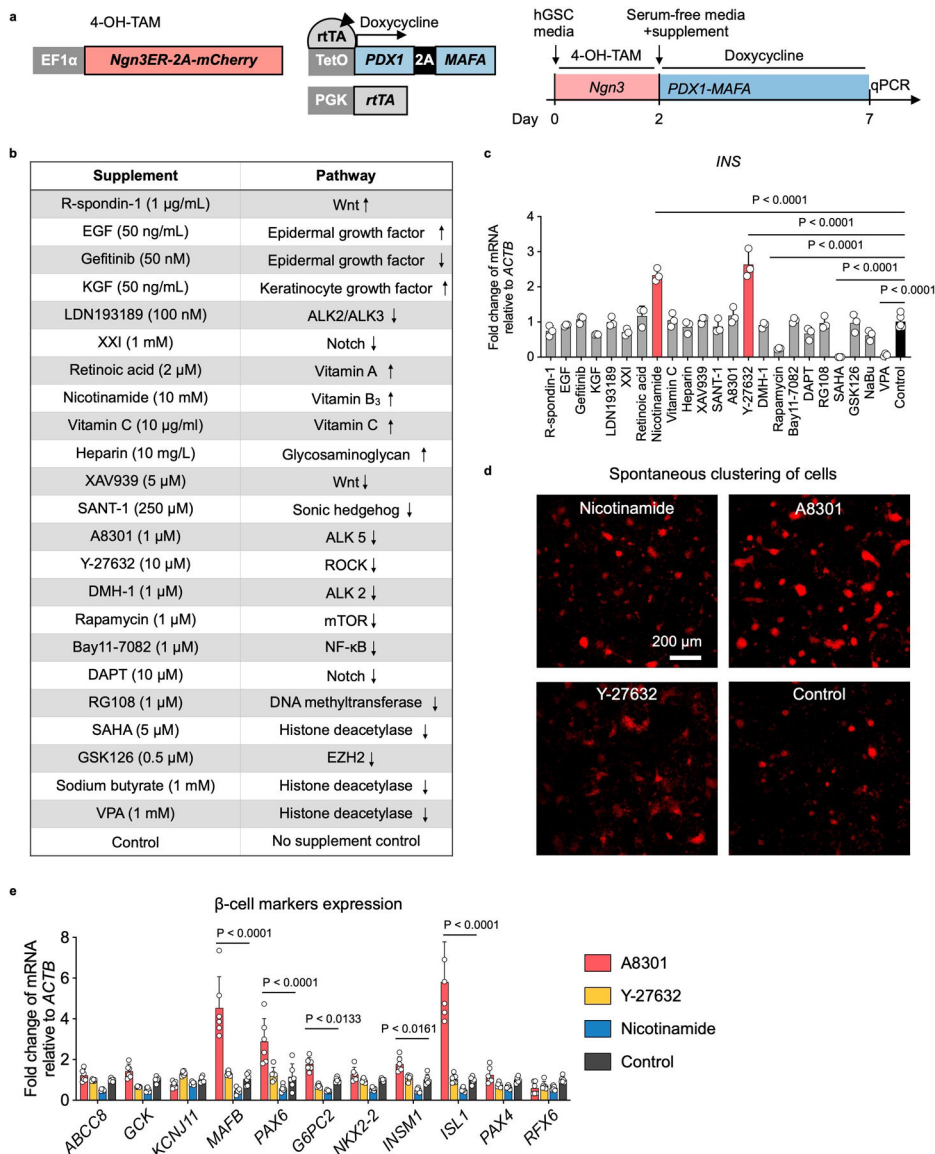
Extended Data Fig. 2 |. Formulating chemically defined serum-free medium for GINS organoid differentiation.

a, Experimental design for the supplement screen. *Ngn3ER*: fusion gene in which NGN3 activity was induced by 4-OH-TAM. Polycistronic PDX1 and MAFA co-expression was controlled by rtTA-TetO and activated by the addition of Doxycycline in the culture medium. mCherry was co-expressed with Ngn3ER in the cell line. Ngn3 was activated from day 0 to day 2. Culture medium was switched to a basal serum-free medium (advanced

DMEM/F12, 10 mM HEPES, 1X GlutaMAX, 1X B-27, 1X N-2, and 500 µM N-Acetyl-L-Cysteine) on day 2 with addition of a single supplement and Doxycycline. **b**, The list of supplements that were screened and the pathways they targeted. Up and down arrows indicate agonists or antagonists, respectively. **c**, Relative expression of *INS* mRNA on day-7 post differentiation in comparison with no supplement control. N = 3 (treatments) or 5 (control) independent samples. Nicotinamide and Y-27632 treatment significantly up-regulated *INS*. **d**, Spontaneous clustering of cells was evaluated by mCherry live imaging on day-7 post differentiation. Select conditions were shown. A8301 treatment had the most observable clustering effect on the nascent GINS cells. Repeated independently 3 times with similar results. **e**, Relative expression of β-cell markers measured on day-7 post differentiation in comparison with no supplement control. N = 6 independent samples. **c**, **e**, Data presented as mean ± s.d.; one-way ANOVA (**c**), or two-way ANOVA (**e**) with Holm–Sidak's multiple comparisons test.
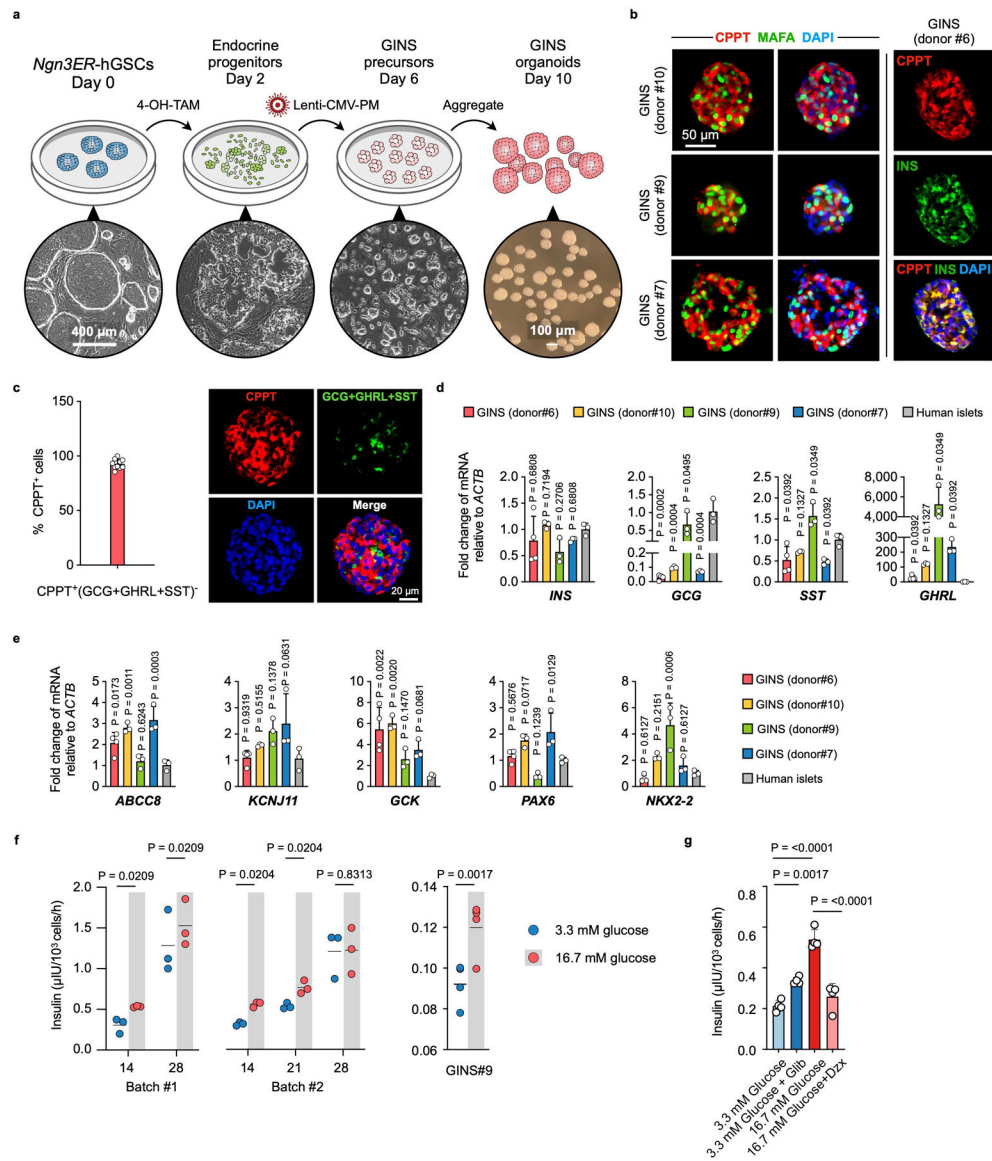
Extended Data Fig. 3 |. Molecular and functional characterization of GINS organoids derived from multiple donors.

a, Schematic diagram and representative images of cells at key stages in GINS organoid formation. *Ngn3ER*-hGSCs: human gastric stem cells that incorporated a *Ngn3* and estrogen receptor (*ER*) fusion gene (*Ngn3ER*); 4-OH-TAM: 4-OH Tamoxifen; Lenti-CMV-PM, lentiviral integration of a polycistronic *Pdx1-Mafa* co-expression cassette. **b**, Representative immunofluorescent staining of corpus GINS organoids derived from three different donors, and co-localization of INS and CPPT in GINS cells. **a**, **b**, Repeated independently 3 times with similar results. **c**, To assess CPPT[+] mono-hormonal cells, a cocktail of GCG, SST and GHRL antibodies were stained together with CPPT in day-21 GINS organoids. Right panel shows immunofluorescent staining of CPPT (red) and a combination of GCG, GHRL and SST (green). left panel shows quantification of mono-hormonal CPPT^{+} cells (n = 10 organoids from donor #6). **d**, Relative expression of endocrine hormone genes including *INS*, *GCG*, *SST,* and *GHRL* in day-18 GINS organoids derived from four different donors

in comparison with human islets. n = 4 (donor#6) or 3 (donor#7, #9, #10, or islet donors) separate batches of samples for each donor. **e**, Relative expression of key β-cell markers in GINS organoids derived from different donors in comparison with human islets. n = 4 (donor#6) or 3 (donor#7, #9, #10, or islet donors) separate batches of samples for each donor. **f**, Glucose-stimulated insulin secretion of GINS organoids at different time points (n = 3 independent samples from donor #6 for each batch of differentiation) or donor #9 (n = 3 independent samples, day-18). **g**, Insulin secretion of day-18 GINS organoids from donor #6 incubated with the indicated concentrations of glucose with or without 10 nM glibenclamide (Glib) or 0.5 mM diazoxide (Dzx) as indicated (n = 4 independent samples). **c-g**, Data presented as mean ± s.d.; one-way ANOVA (**d**, **e**, **g**) or repeated-measures two-way ANOVA with Holm–Sidak's multiple comparisons test for different time points (**f**) or one-tailed paired t-test for donor#9 (**f**).
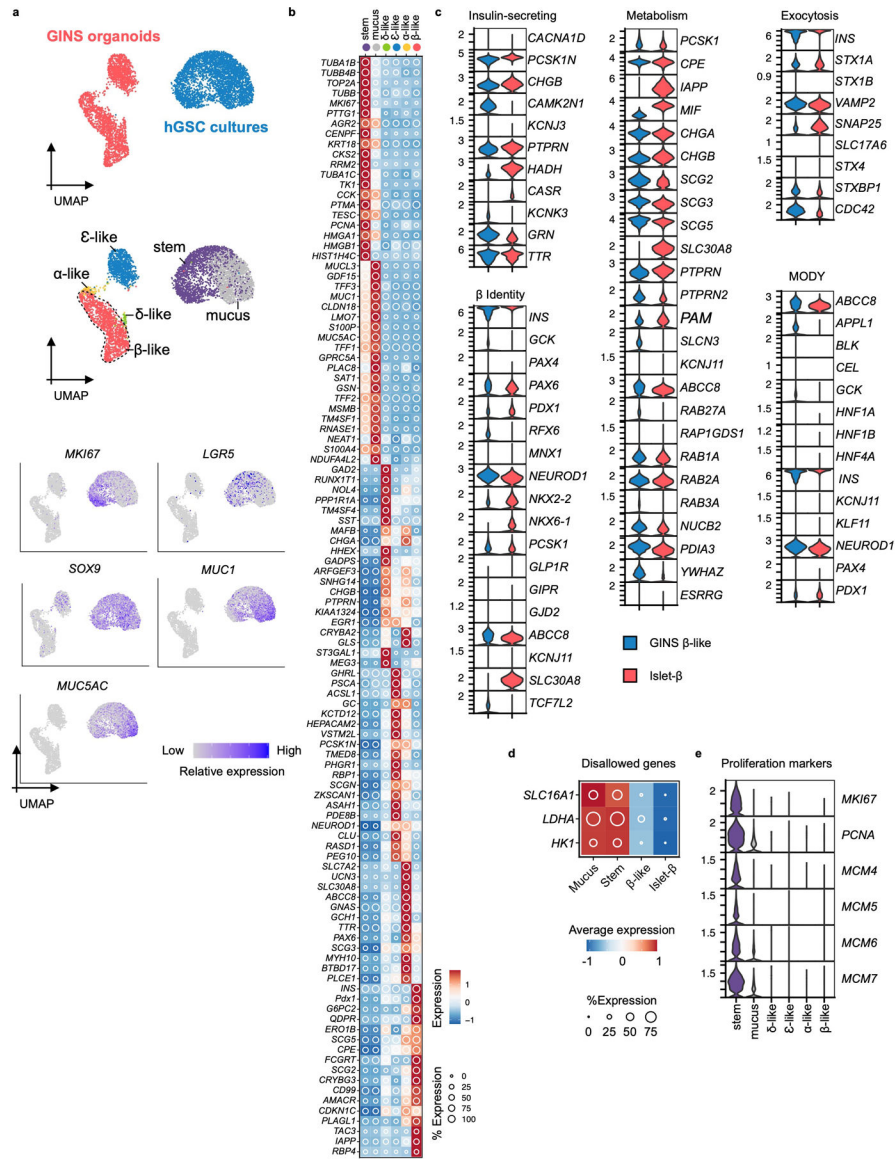
Extended Data Fig. 4 |. Characterizing GINS organoid cells with scRNA-seq.

a, Top UMAP, cells sampled from hGSC cultures (blue, n = 1, donor #6) or GINS organoids (red, n = 1, donor #6); middle UMAP, hGSC cultures included both stem cells (stem) and mucus-secreting cells (mucus) spontaneously differentiated from hGSCs. GINS organoids contained four endocrine cell types. Cells are colored according to cell types; bottom UMAP, relative expression of cell type-specific markers. **b**, Relative expression of endocrine cell type-specific markers. The shading displays scaled average gene expression, and diameter denotes fractional expression. **c**, Comparison of GINS β-like cells (n = 2 independent batch of organoids, one representative batch shown, donor #6) and islet β-cells (n = 4 independent donors, an integration of all samples) in expression profiles of key genes for β-cell function, identity, metabolism, and exocytosis. MODY: Maturity Onset Diabetes of the Young. **d**, Relative expression of disallowed genes in the indicated cell types (n = 1, donor #6). **e**, Violin plots showing the expression levels of proliferative markers in the indicated cell types (n = 1, donor #6).
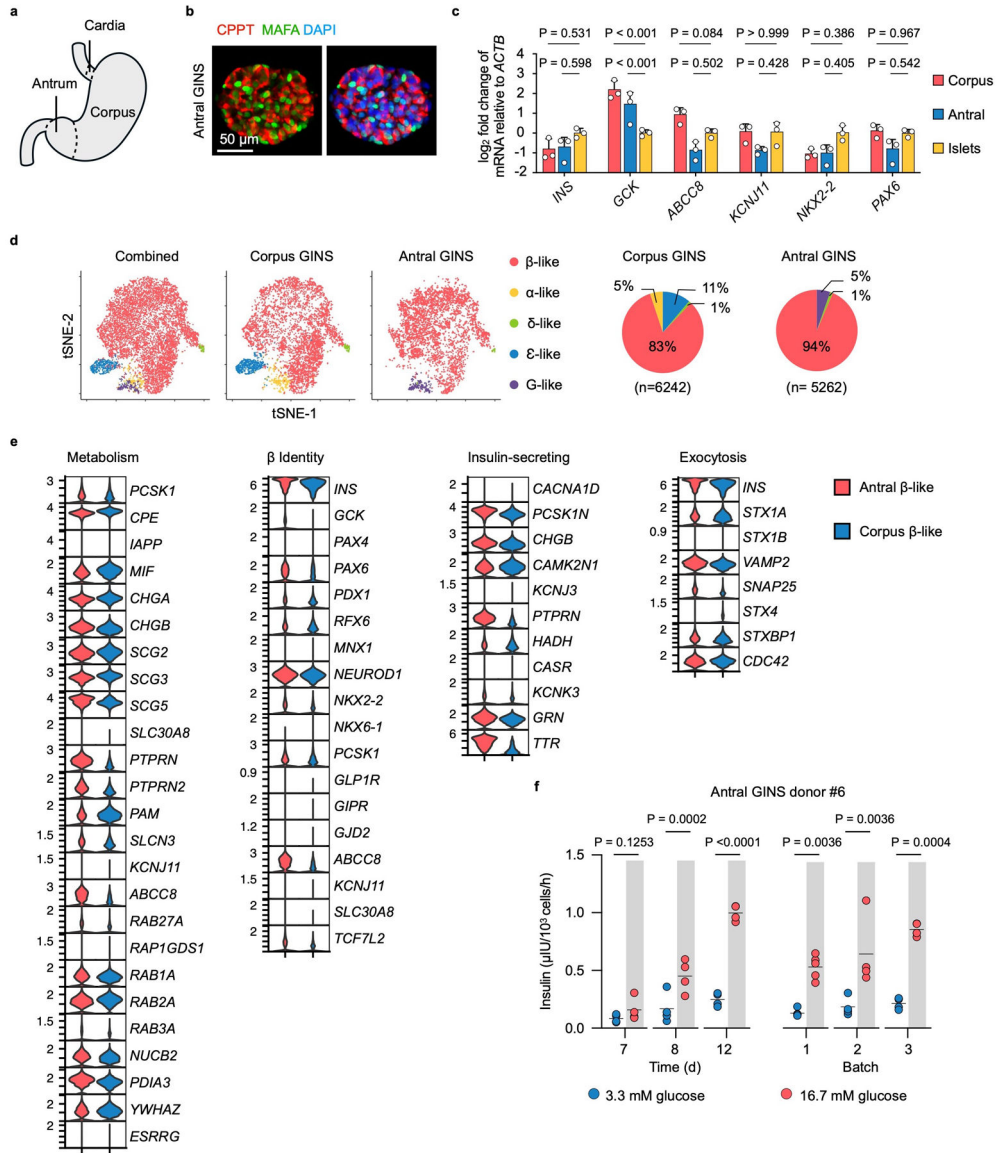
Extended Data Fig. 5 |. scRNA-seq comparison of GINS organoids derived from human antrum vs corpus stomach.

a, Diagram of human stomach. **b**, Immunofluorescence of antral GINS organoid (donor#6) stained for CPPT and MAFA. Repeated independently 5 times with similar results. **c**, Comparison of corpus and antral GINS organoids (both from donor#6) in the expression of β-cell marker genes. n=3 independent experiments. Data presented as mean ± s.d.; one-way ANOVA with Dunnett multiple comparisons test comparing GINS with islets. **d**, t-distributed stochastic neighbor embedding (t-SNE) plots of integrated corpus and antral GINS organoids. Cells are colored according to cell types. G-like: G-like cells that expressed gastrin (*GAST*). Pie charts indicate cell-type proportions. **e**, Comparison of antral and corpus GINS β-like cells expression profiles of key genes for β-cell function and identity. Red, antral GINS β-like cells; Blue, corpus GINS β-like cells. **f**, Glucose-stimulated insulin secretion of antral GINS organoids at different time points (days post differentiation) or from different batches. n=4 independent groups of GINS organoids for the time course
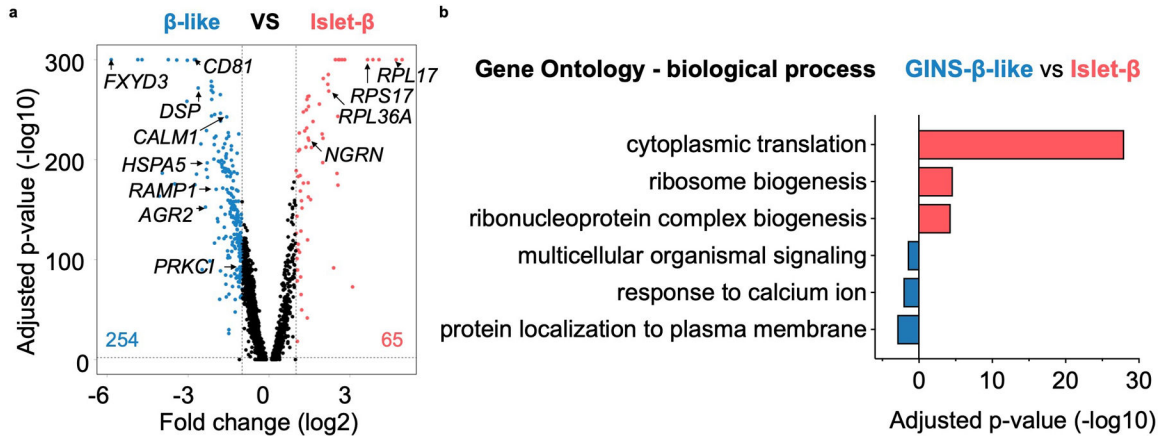
**Extended Data Fig. 6 |. GINS organoids are not fully mature.**

a, Volcano plot comparing gene expression of GINS β-like cells (n = 2 independent batch of organoids, one representative batch is shown, donor #6) versus islet β cells (n = 4 independent donors, an integration of all samples) identified in Fig. 3a. The number of differentially expressed genes (DEGs) enriched in either cell group is shown in the plot. Threshold of DEGs: adjusted-P < 0.01 and $\log_2$ fold-change > 1. P-value calculated by Wilcoxon Rank Sum test and adjusted based on Bonferroni correction. **b**, Gene Ontology (GO) analysis of DEGs enriched in GINS β-like cells (blue) or islet β-cells (red). P-value calculated by hypergeometric distribution followed by Benjamini-Hochberg adjustment.
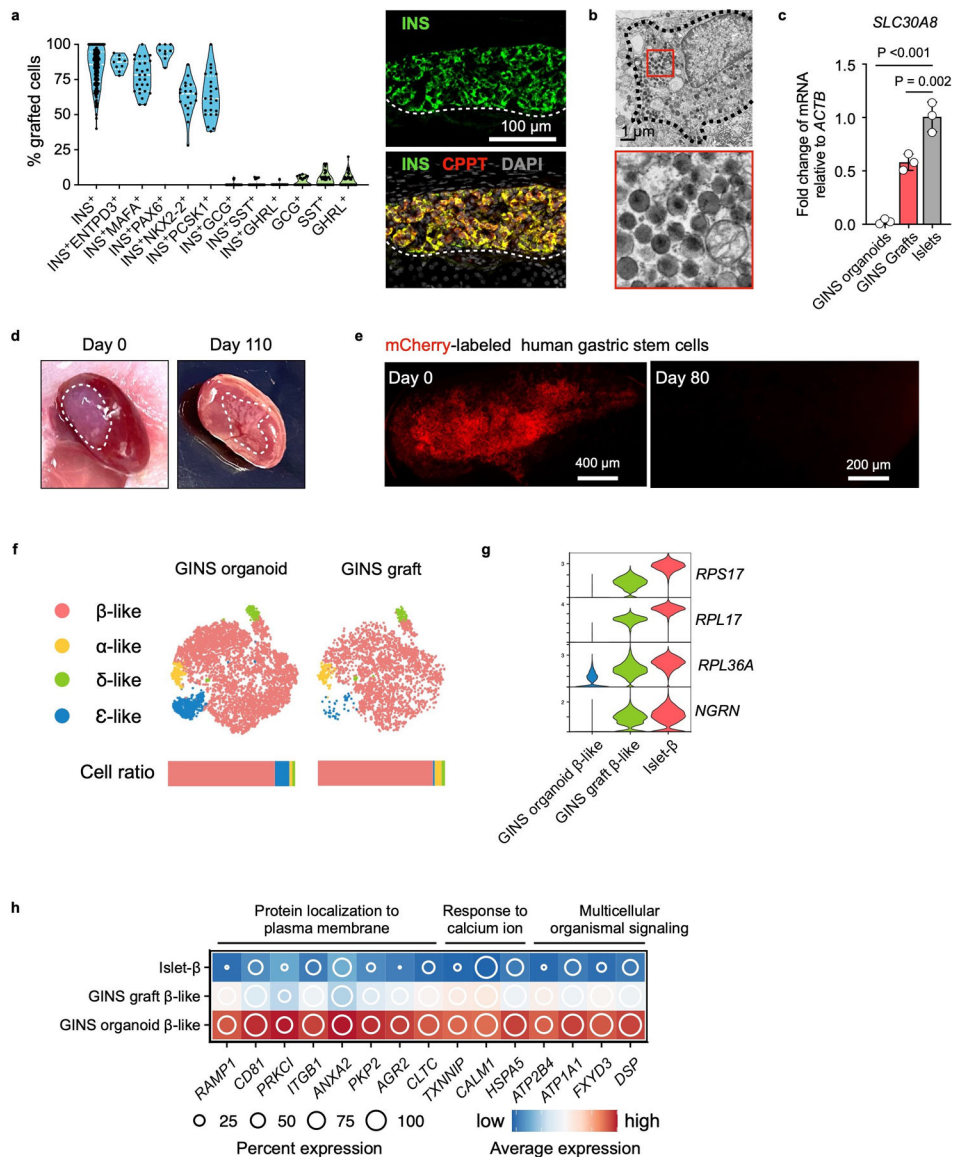
Extended Data Fig. 7 |. Phenotypic characterization of GINS grafts.

a, Quantification from immunofluorescent staining of marker proteins, n = 3 independent experiments. Representative image showing co-expression of INS and CPPT in the GINS graft. **b**, Electron microscopy imaging of GINS graft. The electron-dense core granules were partially condensed. Repeated independently 3 times with similar results. **c**, *SLC30A8* relative expression levels in GINS organoids, GINS grafts, and human islets. n=3 independent groups of GINS organoids, independent GINS grafts from different mice, or independent human islets from different donors. Data presented as mean ± s.d.; one-way ANOVA with Dunnett multiple comparisons test comparing GINS with islets. **d**, Images of the kidney from mice transplanted with GINS cells on day 0 and day 110 post transplantation. **e**, mCherry-labeled hGSCs (0.5×10^6) transplanted under the renal capsule and visualized under fluorescent microscope on day 0 and day 80 post transplantation. No Cherry$^+$ cells were found at day 80. Repeated independently 5 times with similar results. **f**,

tSNE projection of integrated GINS organoids and grafts. Cells are colored according to cell types. Horizontal bars indicate cell type ratios. **g**, Violin plots showing the expression levels of select ribonucleoproteins. **h**, Relative expression of select genes in the pathways elevated in cultured GINS β-like cells compared with human islet-β cells.
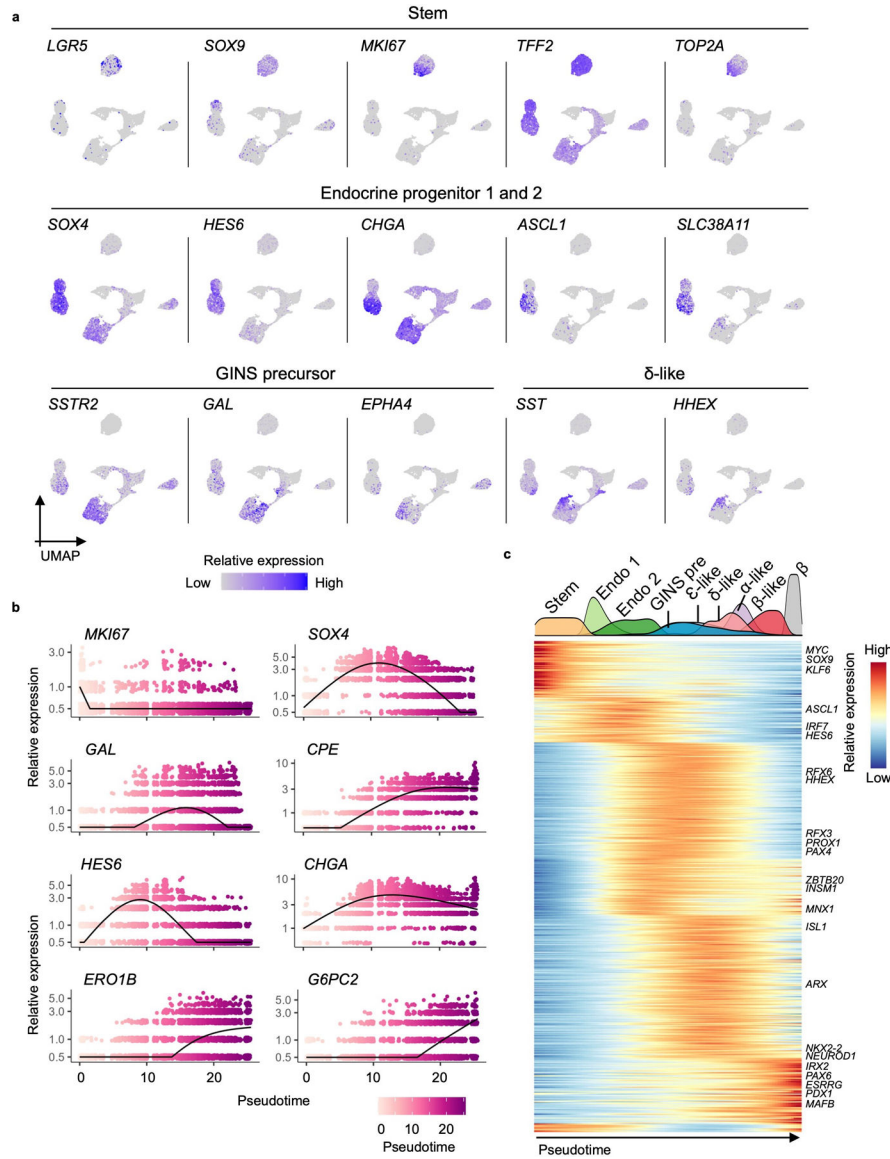
Extended Data Fig. 8 |. Dynamic gene and signaling pathway activations in hGSC differentiation to GINS organoid.

a, Relative expression levels of cell type-specific markers in UMAP. **b**, Expression of select genes shown along pseudotime in GINS organoid formation. Each dot represents a cell. **a**, **b**, n = 1, donor #6. **c**, Heat map showing transcription factor expression clusters along the pseudotime trajectory from hGSCs to GINS organoid cells (n = 1, donor #6) and islet β cells (n = 1, donor #1). Density plot on the top showing cell populations along pseudotime. Stem: hGSCs; Endo 1: endocrine progenitors 1; Endo 2: endocrine progenitors 2; GINS pre: GINS precursors.
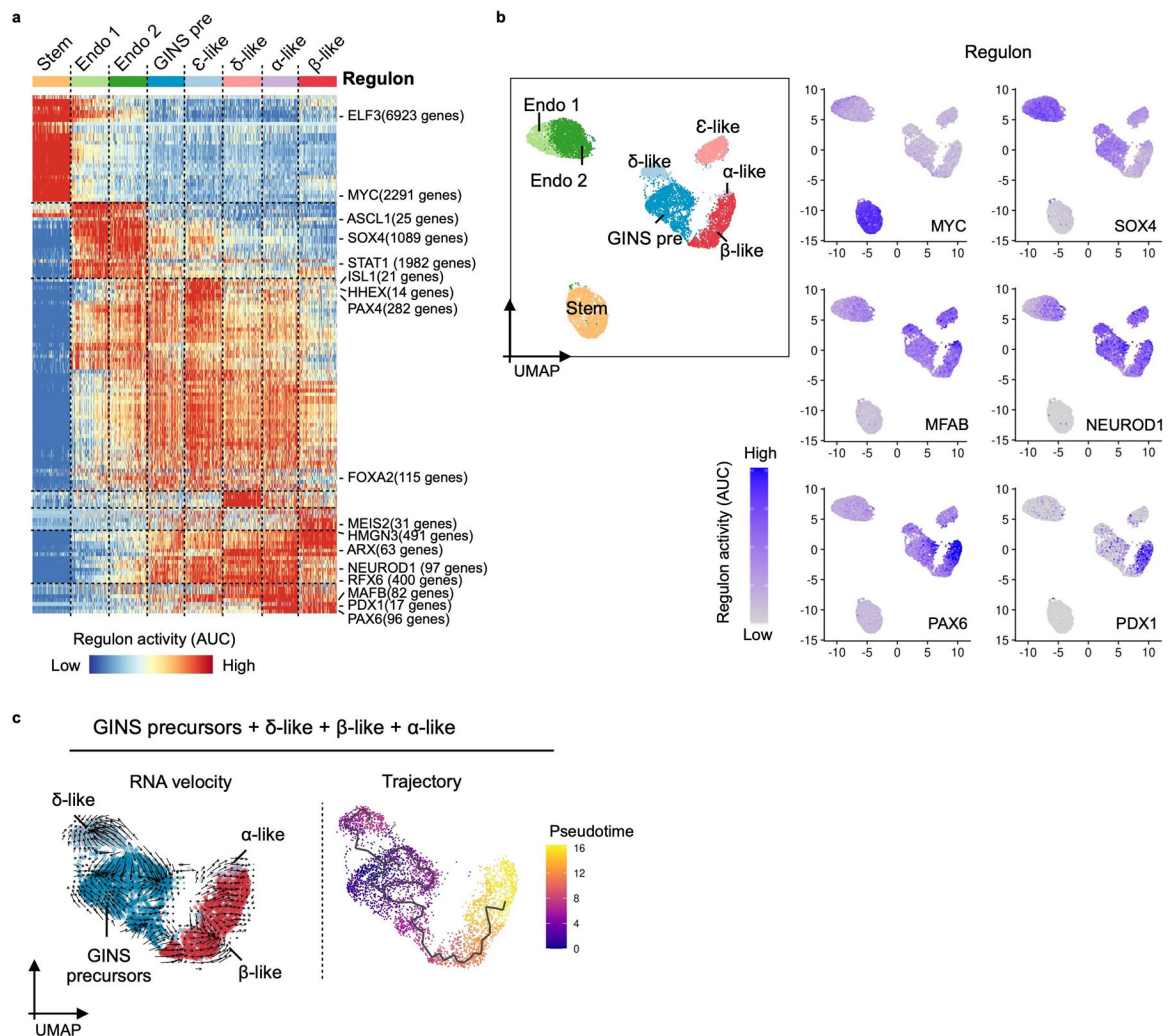
Extended Data Fig. 9 |. Characterization of the developmental path of GINS organoids.
a, Heatmap showing waves of transcription factor regulon activations. Key regulons are labeled on the right with the number of their predicted target genes. Stem: hGSCs; Endo 1: endocrine progenitors 1; Endo 2: endocrine progenitors 2; GINS pre: GINS precursors. **b**, Select regulon activity overlaid on UMAP. **c**, RNA velocity and pseudotime trajectory analysis in UMAP showing the developmental path from GINS precursors to endocrine cells in GINS organoids. **a, b**, n = 1, donor #6.

Supplementary Material

Refer to Web version on PubMed Central for supplementary material.

Acknowledgment

Data availability

Sequencing data that support the findings of this study have been deposited in the GEO under accession code GSE205766. Previously published human islet scRNA-seq data (donors #1, #2, #3, #4 and #9)[30] that we reanalyzed in this study are available under accession code GSE114297[30]. Source data are provided with this study. All other data supporting the findings of this study are available from the corresponding author on reasonable request.

References

1. Gehart H & Clevers H Tales from the crypt: new insights into intestinal stem cells. Nat Rev Gastroenterol Hepatol 16, 19–34, doi:10.1038/s41575-018-0081-y (2019). [PubMed: 30429586]

2. Wells JM & Spence JR How to make an intestine. Development 141, 752–760, doi:10.1242/dev.097386 (2014). [PubMed: 24496613]

3. Santos AJM, Lo YH, Mah AT & Kuo CJ The Intestinal Stem Cell Niche: Homeostasis and Adaptations. Trends Cell Biol 28, 1062–1078, doi:10.1016/j.tcb.2018.08.001 (2018). [PubMed: 30195922]

4. Sugimoto S et al. An organoid-based organ-repurposing approach to treat short bowel syndrome. Nature 592, 99–104, doi:10.1038/s41586-021-03247-2 (2021). [PubMed: 33627870]

5. Nikolaev M et al. Homeostatic mini-intestines through scaffold-guided organoid morphogenesis. Nature 585, 574–578, doi:10.1038/s41586-020-2724-8 (2020). [PubMed: 32939089]

6. Meran L et al. Engineering transplantable jejunal mucosal grafts using patient-derived organoids from children with intestinal failure. Nat Med 26, 1593–1601, doi:10.1038/s41591-020-1024-z (2020). [PubMed: 32895569]

7. Egozi A et al. Insulin is expressed by enteroendocrine cells during human fetal development. Nat Med 27, 2104–2107, doi:10.1038/s41591-021-01586-1 (2021). [PubMed: 34887578]

8. Talchai C, Xuan S, Kitamura T, DePinho RA & Accili D Generation of functional insulin-producing cells in the gut by Foxo1 ablation. Nat Genet 44, 406–412, S401, doi:10.1038/ng.2215 (2012). [PubMed: 22406641]

9. Wang X et al. Cloning and variation of ground state intestinal stem cells. Nature 522, 173–178, doi:10.1038/nature14484 (2015). [PubMed: 26040716]

10. Ariyachet C et al. Reprogrammed Stomach Tissue as a Renewable Source of Functional beta Cells for Blood Glucose Regulation. Cell Stem Cell 18, 410–421, doi:10.1016/j.stem.2016.01.003 (2016). [PubMed: 26908146]

11. Chen YJ et al. De novo formation of insulin-producing "neo-beta cell islets" from intestinal crypts. Cell Rep 6, 1046–1058, doi:10.1016/j.celrep.2014.02.013 (2014). [PubMed: 24613355]

12. Bouchi R et al. FOXO1 inhibition yields functional insulin-producing cells in human gut organoid cultures. Nat Commun 5, 4242, doi:10.1038/ncomms5242 (2014). [PubMed: 24979718]

13. Warshauer JT, Bluestone JA & Anderson MS New Frontiers in the Treatment of Type 1 Diabetes. Cell Metab 31, 46–61, doi:10.1016/j.cmet.2019.11.017 (2020). [PubMed: 31839487]

14. Zhou Q & Melton DA Pancreas regeneration. Nature 557, 351–358, doi:10.1038/s41586-018-0088-0 (2018). [PubMed: 29769672]

15. Brusko TM, Russ HA & Stabler CL Strategies for durable beta cell replacement in type 1 diabetes. Science 373, 516–522, doi:10.1126/science.abh1657 (2021). [PubMed: 34326233]

16. Ramzy A et al. Implanted pluripotent stem-cell-derived pancreatic endoderm cells secrete glucose-responsive C-peptide in patients with type 1 diabetes. Cell Stem Cell 28, 2047–2061 e2045, doi:10.1016/j.stem.2021.10.003 (2021). [PubMed: 34861146]

17. Sneddon JB et al. Stem Cell Therapies for Treating Diabetes: Progress and Remaining Challenges. Cell Stem Cell 22, 810–823, doi:10.1016/j.stem.2018.05.016 (2018). [PubMed: 29859172]

18. Millman JR & Pagliuca FW Autologous Pluripotent Stem Cell-Derived beta-Like Cells for Diabetes Cellular Therapy. Diabetes 66, 1111–1120, doi:10.2337/db16-1406 (2017). [PubMed: 28507211]

19. Barker N et al. Lgr5(+ve) stem cells drive self-renewal in the stomach and build long-lived gastric units in vitro. Cell Stem Cell 6, 25–36, doi:10.1016/j.stem.2009.11.013S1934-5909(09)00618-3 [pii] (2010). [PubMed: 20085740]

20. Barker N et al. Identification of stem cells in small intestine and colon by marker gene Lgr5. Nature 449, 1003–1007, doi:10.1038/nature06196 (2007). [PubMed: 17934449]

21. Sato T et al. Single Lgr5 stem cells build crypt-villus structures in vitro without a mesenchymal niche. Nature 459, 262–265, doi:nature07935 [pii]10.1038/nature07935 (2009). [PubMed: 19329995]

22. Sato T et al. Long-term expansion of epithelial organoids from human colon, adenoma, adenocarcinoma, and Barrett's epithelium. Gastroenterology 141, 1762–1772, doi:10.1053/j.gastro.2011.07.050 (2011). [PubMed: 21889923]

23. Zhou Q, Brown J, Kanarek A, Rajagopal J & Melton DA In vivo reprogramming of adult pancreatic exocrine cells to beta-cells. Nature 455, 627–632, doi:10.1038/nature07314 (2008). [PubMed: 18754011]

24. Hickey RD et al. Generation of islet-like cells from mouse gall bladder by direct ex vivo reprogramming. Stem Cell Res 11, 503–515, doi:10.1016/j.scr.2013.02.005 (2013). [PubMed: 23562832]

25. Li W et al. Long-term persistence and development of induced pancreatic beta cells generated by lineage conversion of acinar cells. Nat Biotechnol 32, 1223–1230, doi:10.1038/nbt.3082nbt.3082 [pii] (2014). [PubMed: 25402613]

26. Lee J et al. Expansion and conversion of human pancreatic ductal cells into insulin-secreting endocrine cells. Elife 2, e00940, doi:10.7554/eLife.00940 (2013). [PubMed: 24252877]

27. Furuyama K et al. Diabetes relief in mice by glucose-sensing insulin-secreting human alpha-cells. Nature 567, 43–48, doi:10.1038/s41586-019-0942-8 (2019). [PubMed: 30760930]

28. Johansson KA et al. Temporal control of neurogenin3 activity in pancreas progenitors reveals competence windows for the generation of different endocrine cell types. Dev Cell 12, 457–465 (2007). [PubMed: 17336910]

29. Duckworth WC, Bennett RG & Hamel FG Insulin degradation: progress and potential. Endocr Rev 19, 608–624, doi:10.1210/edrv.19.5.0349 (1998). [PubMed: 9793760]

30. Xin Y et al. Pseudotime Ordering of Single Human beta-Cells Reveals States of Insulin Production and Unfolded Protein Response. Diabetes 67, 1783–1794, doi:10.2337/db18-0365 (2018). [PubMed: 29950394]

31. Pullen TJ et al. Identification of genes selectively disallowed in the pancreatic islet. Islets 2, 89–95, doi:10.4161/isl.2.2.11025 (2010). [PubMed: 21099300]

32. Muraro MJ et al. A Single-Cell Transcriptome Atlas of the Human Pancreas. Cell Syst 3, 385–394 e383, doi:10.1016/j.cels.2016.09.002 (2016). [PubMed: 27693023]

33. Busslinger GA et al. Human gastrointestinal epithelia of the esophagus, stomach, and duodenum resolved at single-cell resolution. Cell Rep 34, 108819, doi:10.1016/j.celrep.2021.108819 (2021). [PubMed: 33691112]

34. Saunders DC et al. Ectonucleoside Triphosphate Diphosphohydrolase-3 Antibody Targets Adult Human Pancreatic beta Cells for In Vitro and In Vivo Analysis. Cell Metab 29, 745–754 e744, doi:10.1016/j.cmet.2018.10.007 (2019). [PubMed: 30449685]

35. Lemaire K et al. Insulin crystallization depends on zinc transporter ZnT8 expression, but is not required for normal glucose homeostasis in mice. Proc Natl Acad Sci U S A 106, 14872–14877, doi:10.1073/pnas.0906587106 (2009). [PubMed: 19706465]

36. Flannick J et al. Loss-of-function mutations in SLC30A8 protect against type 2 diabetes. Nat Genet 46, 357–363, doi:10.1038/ng.2915 (2014). [PubMed: 24584071]

37. Dwivedi OP et al. Loss of ZnT8 function protects against diabetes by enhanced insulin secretion. Nat Genet 51, 1596–1606, doi:10.1038/s41588-019-0513-9 (2019). [PubMed: 31676859]

38. van der Flier LG & Clevers H Stem cells, self-renewal, and differentiation in the intestinal epithelium. Annu Rev Physiol 71, 241–260, doi:10.1146/annurev.physiol.010908.163145 (2009). [PubMed: 18808327]

39. Yan KS et al. Non-equivalence of Wnt and R-spondin ligands during Lgr5(+) intestinal stem-cell self-renewal. Nature 545, 238–242, doi:10.1038/nature22313 (2017). [PubMed: 28467820]

40. Melton D The promise of stem cell-derived islet replacement therapy. Diabetologia 64, 1030–1036, doi:10.1007/s00125-020-05367-2 (2021). [PubMed: 33454830]

41. Yoshihara E et al. Immune-evasive human islet-like organoids ameliorate diabetes. Nature 586, 606–611, doi:10.1038/s41586-020-2631-z (2020). [PubMed: 32814902]

42. Deuse T et al. Hypoimmunogenic derivatives of induced pluripotent stem cells evade immune rejection in fully immunocompetent allogeneic recipients. Nat Biotechnol 37, 252–258, doi:10.1038/s41587-019-0016-3 (2019). [PubMed: 30778232]

43. Parent AV et al. Selective deletion of human leukocyte antigens protects stem cell-derived islets from immune rejection. Cell Rep 36, 109538, doi:10.1016/j.celrep.2021.109538 (2021). [PubMed: 34407395]

44. Noguchi GM & Huising MO Integrating the inputs that shape pancreatic islet hormone release. Nat Metab 1, 1189–1201, doi:10.1038/s42255-019-0148-2 (2019). [PubMed: 32694675]

Methods-only references

45. Gu W, Colarusso JL, Dame MK, Spence JR & Zhou Q Rapid establishment of human colonic organoid knockout lines. STAR Protoc 3, 101308, doi:10.1016/j.xpro.2022.101308 (2022). [PubMed: 35463469]

46. Huang X Zhou Q Generation of gastirc insulin-secreting organoids from human stomach sample. Protocol Exchange (2023).

47. Gu W et al. SATB2 preserves colon stem cell identity and mediates ileum-colon conversion via enhancer remodeling. Cell Stem Cell, doi:10.1016/j.stem.2021.09.004 (2021).

48. Butler A, Hoffman P, Smibert P, Papalexi E & Satija R Integrating single-cell transcriptomic data across different conditions, technologies, and species. Nat Biotechnol 36, 411–420, doi:10.1038/nbt.4096 (2018). [PubMed: 29608179]

49. McGinnis CS, Murrow LM & Gartner ZJ DoubletFinder: Doublet Detection in Single-Cell RNA Sequencing Data Using Artificial Nearest Neighbors. Cell Syst 8, 329–337 e324, doi:10.1016/j.cels.2019.03.003 (2019). [PubMed: 30954475]

50. Young MD & Behjati S SoupX removes ambient RNA contamination from droplet-based single-cell RNA sequencing data. Gigascience 9, doi:10.1093/gigascience/giaa151 (2020).

51. Trapnell C et al. The dynamics and regulators of cell fate decisions are revealed by pseudotemporal ordering of single cells. Nat Biotechnol 32, 381–386, doi:10.1038/nbt.2859 (2014). [PubMed: 24658644]

52. Qiu X et al. Single-cell mRNA quantification and differential analysis with Census. Nat Methods 14, 309–315, doi:10.1038/nmeth.4150 (2017). [PubMed: 28114287]

53. Qiu X et al. Reversed graph embedding resolves complex single-cell trajectories. Nat Methods 14, 979–982, doi:10.1038/nmeth.4402 (2017). [PubMed: 28825705]

54. La Manno G et al. RNA velocity of single cells. Nature 560, 494–498, doi:10.1038/s41586-018-0414-6 (2018). [PubMed: 30089906]

55. Aibar S et al. SCENIC: single-cell regulatory network inference and clustering. Nat Methods 14, 1083–1086, doi:10.1038/nmeth.4463 (2017). [PubMed: 28991892]

56. Yu G, Wang LG, Han Y & He QY clusterProfiler: an R package for comparing biological themes among gene clusters. OMICS 16, 284–287, doi:10.1089/omi.2011.0118 (2012). [PubMed: 22455463]

57. Wu T et al. clusterProfiler 4.0: A universal enrichment tool for interpreting omics data. Innovation (N Y) 2, 100141, doi:10.1016/j.xinn.2021.100141 (2021).

58. Nair GG et al. Recapitulating endocrine cell clustering in culture promotes maturation of human stem-cell-derived beta cells. Nat Cell Biol 21, 263–274, doi:10.1038/s41556-018-0271-4 (2019). [PubMed: 30710150]

59. Pagliuca FW et al. Generation of functional human pancreatic beta cells in vitro. Cell 159, 428–439, doi:10.1016/j.cell.2014.09.040 (2014). [PubMed: 25303535]
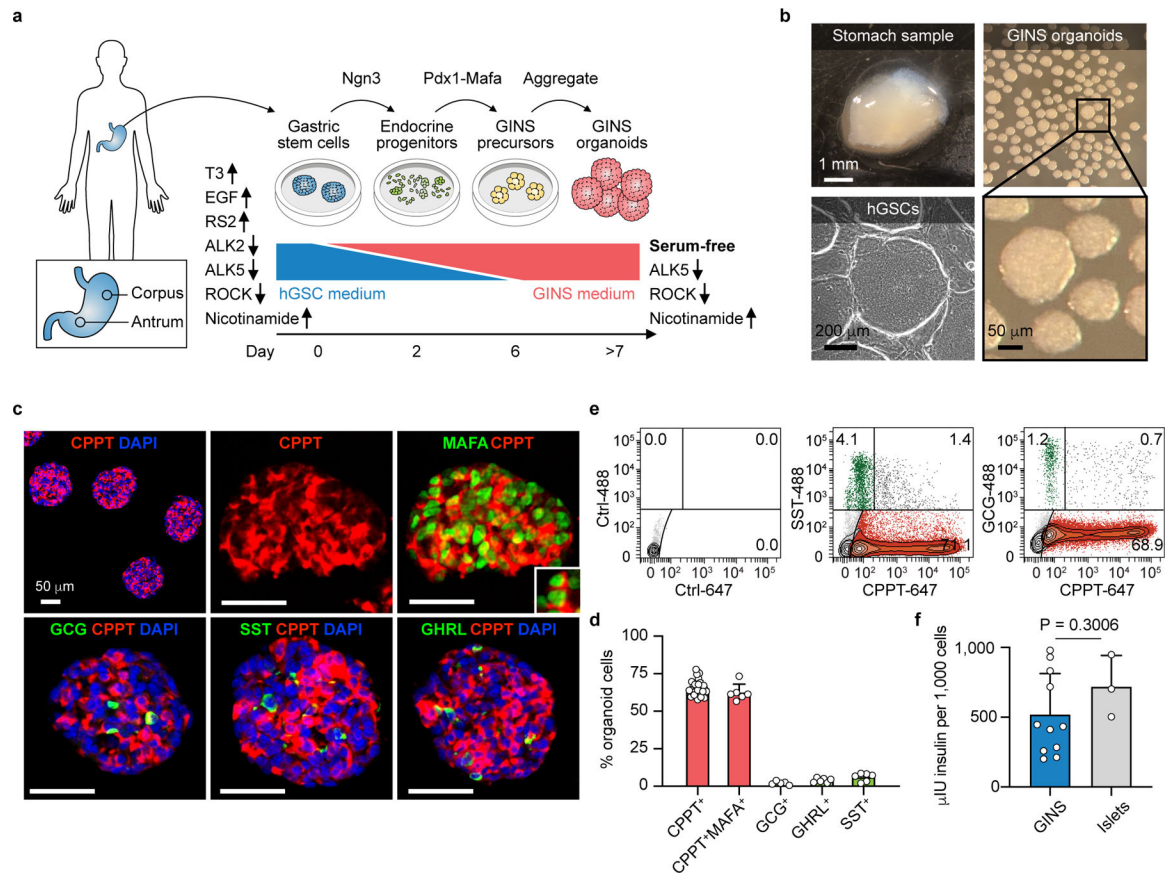
Fig. 1 |. Generation of Gastric Insulin-Secreting (GINS) organoids from human stomach samples.

a, Diagram showing key steps of GINS organoid generation. Medium supplements for hGSC (human gastric stem cell) culture or GINS organoid induction are indicated, with up and down arrows indicating agonists or antagonists, respectively. **b**, Representative images of human stomach samples, hGSC colonies, and GINS organoids. 1000 cells per organoids. **c**, **d**, Immunofluorescent staining and quantification of day-21 GINS organoids for C-peptide (CPPT), MAFA, glucagon (GCG), somatostatin (SST), and ghrelin (GHRL). For CPPT[+] cell quantification, n = 33 independent organoids (donor #6), for other hormone quantification, n = 6 independent organoids (donor #6). **e**, Quantitative flow cytometry of day-21 GINS organoids (donor #10) with negative control. **f**, Insulin content of day-18 GINS organoids (n = 11 different batches of organoids from donor #6) and human islets (n = 3 samples from independent donors). Data are mean ± s.d.; two-tailed unpaired t-test.
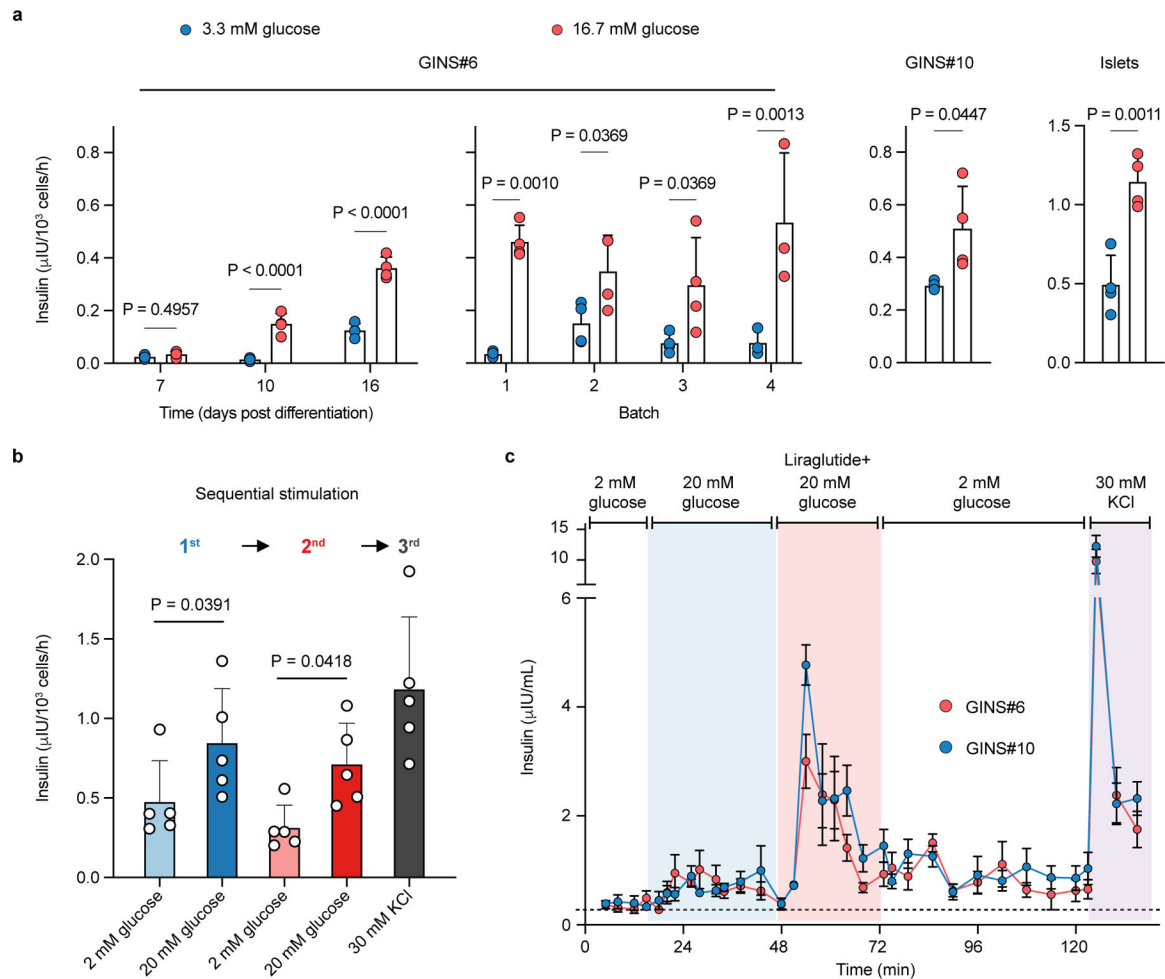
Fig. 2 |. GINS organoids secret human insulin in response to glucose and GLP-1 analogue.
a, Glucose-stimulated insulin secretion of GINS organoids from donor #6 at different time points (days post differentiation, n = 4 independent groups of same batch organoids per time point), from different batches (n = 4 (batch1-3) or n = 3 (batch 4) independent groups of organoids per batch), or from donor #10 (n = 4 independent batches of organoids). For GINS organoids from donor #6, two-way repeated-measures ANOVA with Holm–Sidak's multiple comparisons test. For GINS organoids from donor #10 and islets, one-tailed paired t-test. **b**, Insulin secretion of day-18 GINS organoids in response to sequential glucose challenges and KCl depolarization (n = 5 groups of organoids from donor #6, from two independent experiments). One-way repeated measures ANOVA with Holm–Sidak's multiple comparisons test. **c**, Dynamic glucose-stimulated insulin secretion by perifusion assay of day-21 GINS organoids derived from donor #6 and #10 (n = 4 independent groups of organoids for each donor). **a**, **b**, **c**, Data presented as mean ± s.d.
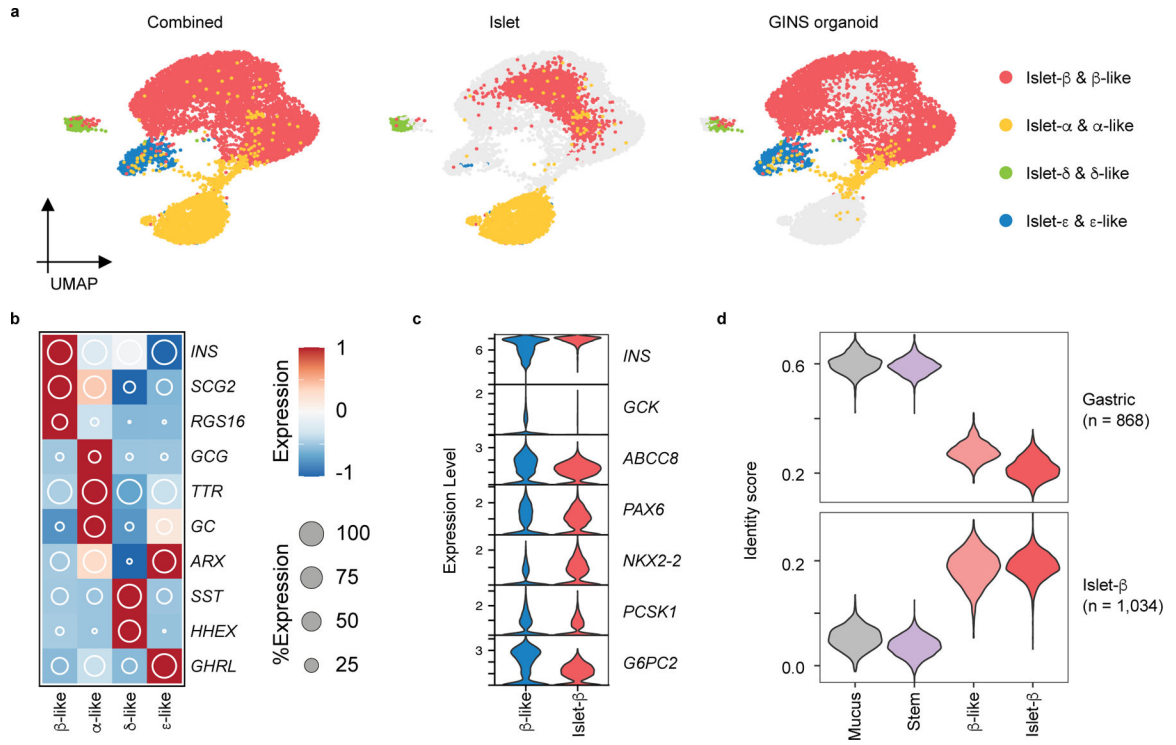
Fig. 3 |. Four endocrine cell types identified in GINS organoids by scRNA-seq.
a, UMAP visualization of integrated GINS organoid (day 21, n = 1, donor #6) and primary human islet single-cell transcriptomes (n = 4 independent donors). **b**, Relative expression of endocrine cell type-specific markers. The shading displays scaled average gene expression, and diameter denotes fractional expression. **c**, Violin plots of key β-cell function and identity markers in GINS β-like and islet β cells. **d**, Cell identity scoring with gastric and β-cell signatures (868 and 1,034 genes, respectively). Mucus: mucus-secreting cells spontaneously differentiated from hGSCs in culture; Stem: hGSCs; β-like: GINS β-like cells; islet-β: islet β-cells.
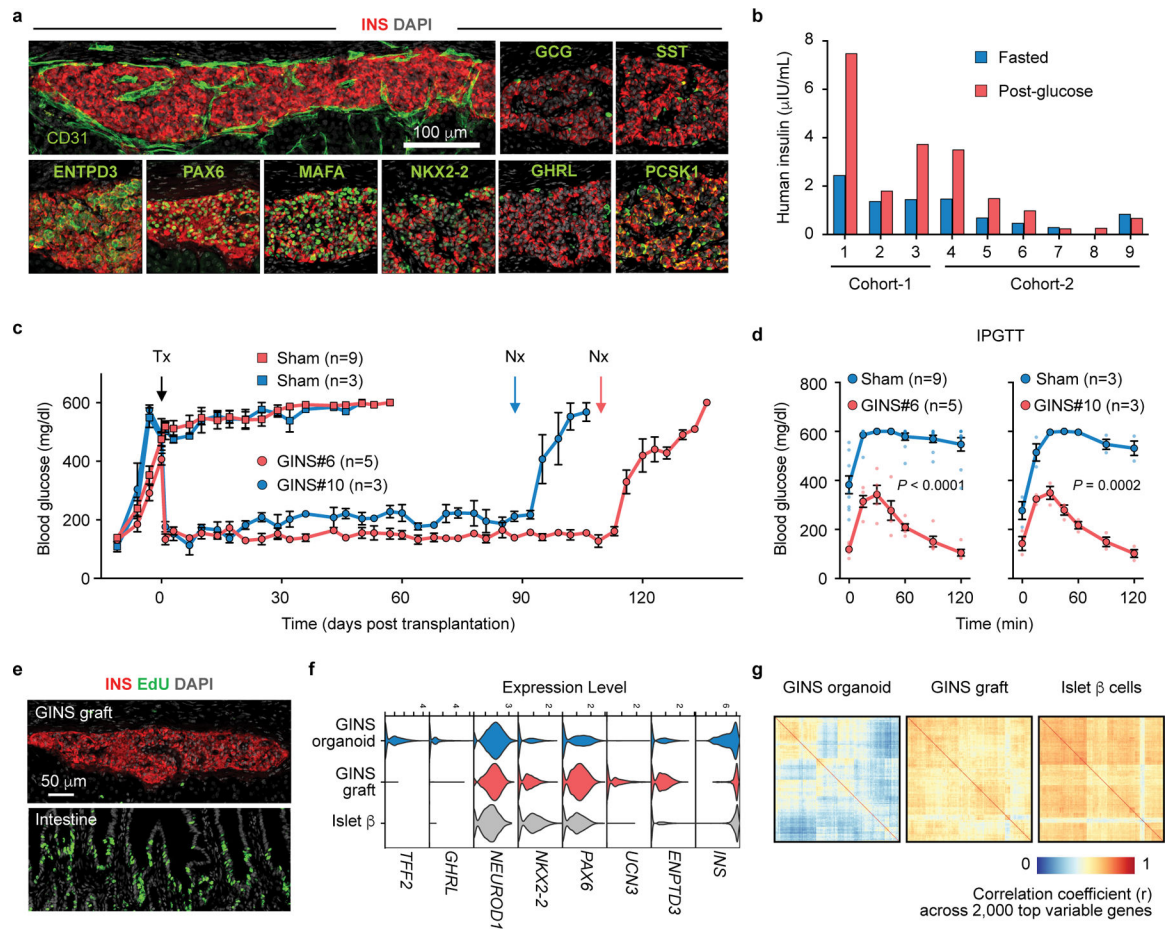
Fig. 4 |. Transplanted GINS organoids secrete human insulin and reversed diabetes in mice.
a, **b**, GINS cells (0.8 x 10^6, corpus donor #6) were transplanted under the renal capsule of non-diabetic NSG mice, which yielded grafts containing CD31$^+$ vascular cells and predominant INS$^+$ cells that co-expressed PAX6, MAFA, NKX2-2, PCSK1, and the mature β cell-associated marker ENTPD3 (6 months post transplantation). A small number of SST$^+$, GCG$^+$, and GHRL$^+$ were also found. Repeated independently 3 times with similar results. (**a**). Human insulin from individual mouse was measured at 7 weeks (cohort-1) and 11 weeks (cohort-2) post transplantation, grafted with different batches of cells, after overnight fasting (blue bar) and 60 minutes after glucose challenge (red bar) (**b**). **c**, **d**, STZ-induced diabetic NSG mice were transplanted with 6–8 million GINS cells from donor #6 (GINS#6, n = 5 independent batches of organoids transplanted into 5 individual mice) or 6 million GINS cells from donor #10 (GINS#10, n = 3 independent batches of organoids transplanted into 3 independent mice) or without transplantation (Sham). Random-fed blood glucose levels (**c**) and intraperitoneal glucose tolerance tests (IPGTT, 2 weeks post transplantation) (**d**) showed significant improvement for both transplanted groups. Data presented as mean ± s.e.m.; two-way repeated-measures ANOVA. Tx: transplantation. Nx: nephrectomy. **e**, 24-hour pulse-chase with EdU revealed no proliferative cells in GINS graft but abundant replicating cells in the intestine of the same engrafted mouse. Repeated independently 3 times with similar results. **f**, Violin plots of select genes in GINS β-like cells before and

after transplantation and comparison with islet β cells. **g,** Assessment of transcriptomic heterogeneity among GINS β-like cells before and after transplantation and among primary human islet β cells with correlation coefficient analysis across 2,000 top variable genes.
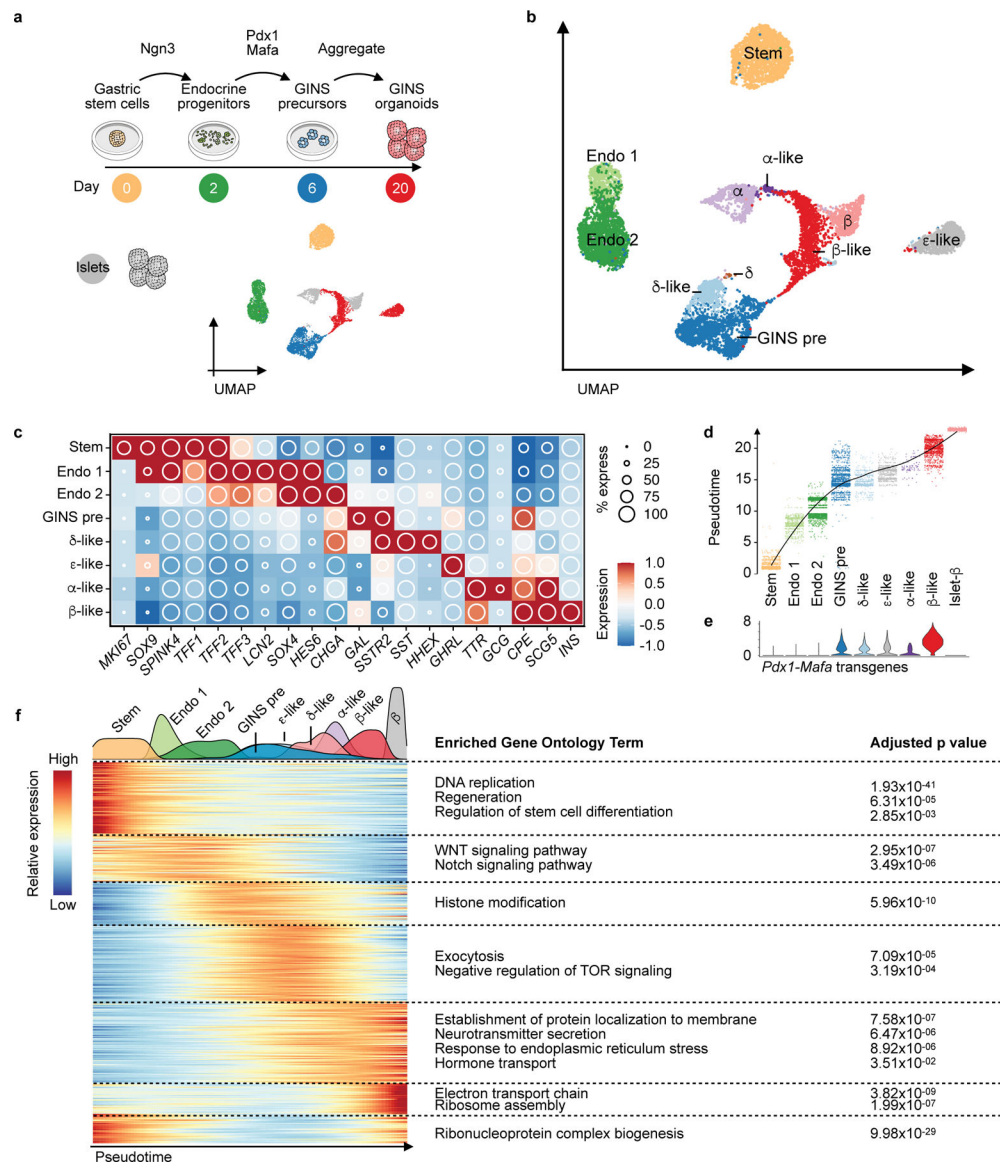
Fig. 5 |. Developmental trajectory of GINS cells.
a, Experimental design of sampling cells with scRNA-seq at key stages of hGSC differentiation to GINS organoids. UMAP showing clustering of hGSCs (day 0, yellow, n = 1, donor #6), endocrine progenitors (day 2, green, n = 1, donor #6), GINS precursors (day 6, blue, n = 1, donor #6), GINS organoids (day 20, red, n = 1, donor #6) and primary human islets (gray, n = 1, donor #1). **b**, UMAP of cell types colored according to their identities. Stem: hGSCs; Endo 1: endocrine progenitors 1; Endo 2: endocrine progenitors 2; GINS pre: GINS precursors. **c**, Relative expression of select markers across cell types. **d**, Pseudotime trajectory analysis of cell types. **e**, Violin plot showing the expression levels of the *Pdx1-Mafa* transgenes in different cell types. **f**, Heat map showing gene-expression clusters along the pseudotime trajectory from hGSCs to GINS cells and human islet β cells. Select significant GO terms enriched in each gene cluster are shown. P-value calculated by hypergeometric distribution followed by Benjamini-Hochberg adjustment.
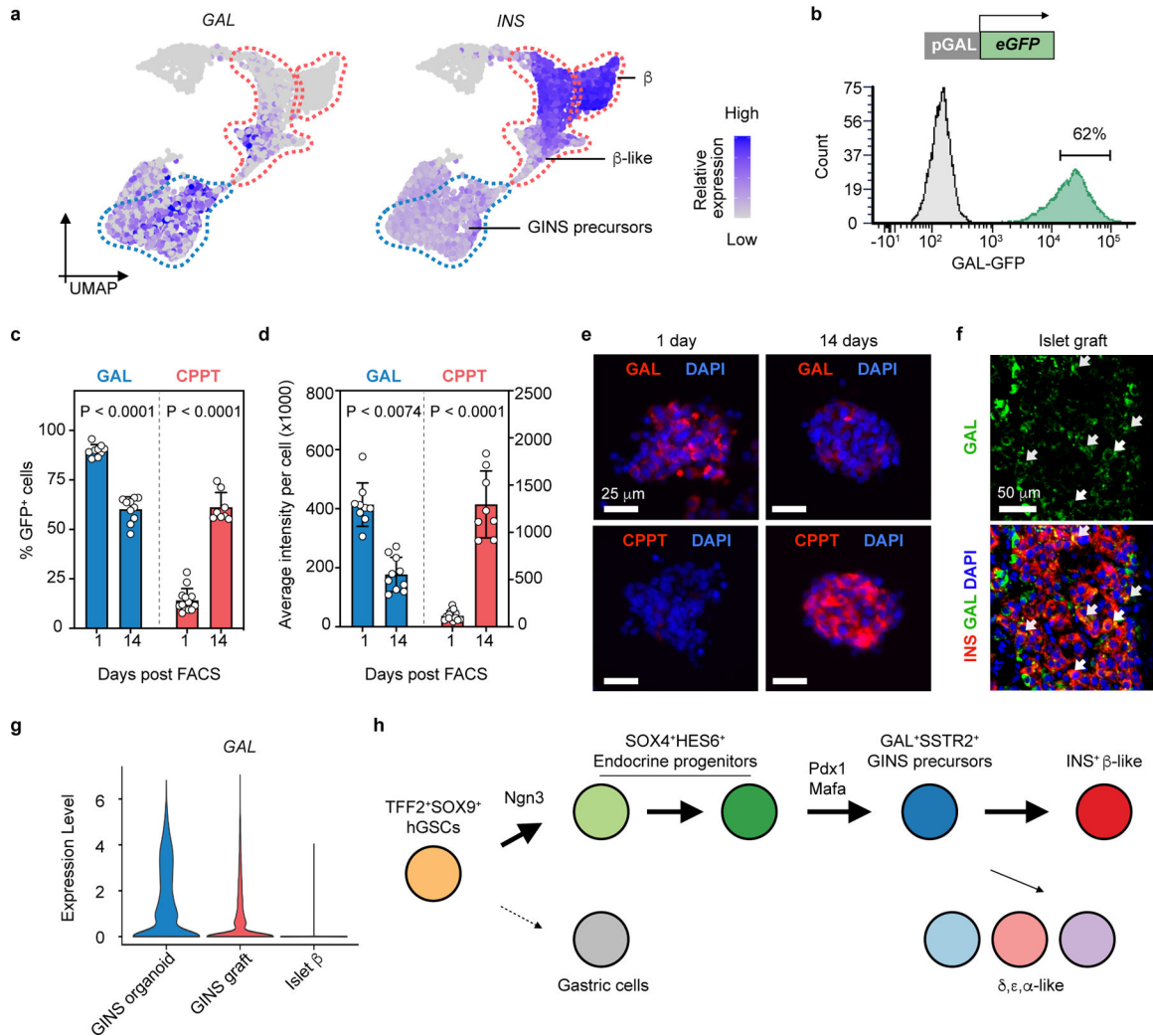
Fig. 6 |. Galanin⁺ precursors give rise to GINS cells.

a, Relative expression of *INS* and *GAL* in GINS precursors, GINS β-like cells and human islet β cells. UMAP subset of Fig. 5b. **b**, Purification of GFP^high GINS precursors differentiated from *GAL-GFP* hGSC reporter line at day 7 post differentiation. **c**, **d**, Quantification of GAL⁺ and CPPT ⁺ cell percentage in organoids and their average staining intensity at day 1 or 14 post sorting. Data presented as mean ± s.d. (GAL⁺ at day 1: n = 9; GAL⁺ at day 14: n = 10; CPPT⁺ at day 1: n = 13; CPPT⁺ at day 14: n = 8; all independent organoids from donor #6); two-way ANOVA with Sidak's multiple comparisons test. **e**, Representative images of immunofluorescent staining for GAL and CPPT at day 1 and day 14 post sorting. **f**, Representative immunofluorescence of GAL and INS in primary human islet grafts in NSG mice. Arrows indicate GAL⁺INS⁺ cells. **g**, Violin plot showing scRNA levels of *GAL* in GINS β-like cells before and after transplantation and in human islet β cells. **h**, Proposed model for GINS organoid formation, with rerouting of the hGSC developmental trajectory by NGN3, PDX1 and MAFA.